PREPARATION OF PYRAMIDAL ZINC OXIDE PARTICLE AS AN ANTIREFLECTIVE

COATING FOR APPLICATION IN SOLAR CELL

by

AMIT BANIK

Presented to the Faculty of the Graduate School of

The University of Texas at Arlington in Partial Fulfillment

of the Requirements

for the Degree of

MASTER OF SCIENCE IN ELECTRICAL ENGINEERING

THE UNIVERSITY OF TEXAS AT ARLINGTON

DECEMBER 2009

ACKNOWLEDGEMENTS

ABSTRACT

PREPARATION OF PYRAMIDAL ZINC OXIDE PARTICLE AS AN ANTIREFLECTIVE

COATING FOR APPLICATION IN THIN FILM SOLAR CELL

AMIT BANIK, M.S.

The University of Texas at Arlington, 2009

Supervising Professor: Meng Tao

There is a lot of research going on in the field of solar cell to increase the energy conversion efficiency. Many new methods have been implemented and new processes and materials have been suggested in the recent past. This research deals with the preparation of pyramidal structure zinc oxide particles as an antireflective coating for polycrystalline and non-silicon solar cell. The process involved a cost effective method that is electrochemical deposition of zinc oxide on silicon mold. The mold, inverted pyramid, is prepared by photolithographic process PECVD silicon nitride as the hard mask and wet etching and then electrochemical deposition is carried to deposit zinc oxide into the molds. The deposition was carried out in a 0.1 mole Zinc nitrate bath at 60ºC using a potentiostat. X-ray diffraction measurement is also carried out to determine verify the deposited zinc oxide.The samples are annealed at different temperature and then reflection and transmission parameters is found using spetrophotometer measurement and it is found to be around 80% transmission. To extract the reflection and transmission zinc oxide is deposited on Indium Tin Oxide(ITO), prepared by

sputtering having a thickness of ~2µm. The bandgap is also calculated from the transmission and reflection data and is found to be 3.4eV. Finally the deposited particles are extracted and SEM characterization is done on the particles.

TABLE OF CONTENTS

LIST OF ILLUSTRATIONS

Figure   Page

ix

x

LIST OF TABLES

xi

CHAPTER 1

HISTORY, MARKET AND FUTURE OF PHOTOVOLTAIC CELL TECHNOLOGY

1.1 Brief history of Solar cell

The history of solar technology spans back to 7th century BC when magnifying glass was used to concentrate sun's rays. However the timeline for real development for the solar cell technology started from 1767 when a Swiss scientist Horace de Saussure built the world's first solar collector and later used to cook food. The photovoltaic effect was discovered by the French scientist Edmond Becquerel while experimenting with the electrolytic cell made up of two meta electrodes placed in a conducting solution; the electricity generation increased when exposed to light. In 1883 an American inventor described the first solar cells made from selenium wafer. In 1954 Gerald Pearson, Daryl Chapin and Calvin Fuller Developed first Silicon Photovoltaic(PV) cell at Bell Labs. The Bell labs produced solar cell which had an efficiency of 4% and later achieved 11% efficiency. Despite the uncertainty in commercializing the silicon solar cell in 1950s and 60s, it was used successfully in powering satellites and hence it became the accepted energy source for space application. In 1972 the Institute of Energy Conversion is established at the University of Delaware to perform research and development on thin-film PV and solar thermal systems and becoming the world's first laboratory dedicated to PV research and development and Solar One of the world's first PV powered residencies was built by the University of Delaware. Following that in 1977 the U.S. Department of Energy launches the Solar Energy Research Institute "National Renewable Energy Laboratory"(NREL) a federal government facility dedicated to harnessing power from the sun. In 1980 ARCO solar becomes the first company to produce more than 1 megawatt of Photovoltaic modules in one year. The Florida Solar Energy Center's "Southeast Residential Experiment Station" begins supporting the

1

U.S. Department of Energy's photovoltaics program in the application of system engineering. In the 80's ARCO solar dedicated 6-megawatt photovoltaic substation in central California, also releases the G-4000- the world's first commercial thin film power module and the University of South Wales breaks the 20% efficiency barrier for Silicon Solar cells. In the 1990's University of South Florida develops a 15.9% efficient thin-film photovoltaic cell made of Cadmium Teleride(CdTe). In the 90's there was a advancement in application of solar cell technology in building and airplane, the NREL completed the construction of its "Solar Energy Researchc Facility", which was recognized as the energy efficient of U.S. government buildings worldwide and NREL also developed solar cell made from Gallium Indium Phosphide and Gallium Arsenide which exceeded 30% conversion efficiency. The 'Icare' worlds most advanced solar powered flew over Germany; the wings and the tail surfaces of the Icare were covered by 3000 super-efficient solar cells. Multilayer solar cell was also developed by Spectrolab, Inc. and NREL which converts 32.3 percent of sunlight that hits into electricity and NREL also developed the 18.8 percent efficiency thin-film photovoltaic solar cells.

In 21st century there is a further progress in the solar cell commercialization and application in the terrestrial as well as extraterrestrial application. First Solar started manufacturing solar panels which could produce 100 megawatts of power, International Space Station installs solar panels which became the largest solar power array in space. New thin-film solar modules were developed with higher efficiency and National Aeronautics and Space Administration (NASA) develops solar power aircraft –Helios sets a new world record for non-rocket powered aircraft, more than 18miles high.[1]

The first use of silicon solar cells in an orbiting space satellite was in Vanguard I launched on March 17, 1958. The requirement of the space program generated a industry for solar cells. To obtain the efficiencies of 10 or more consistently contact fingers were introduced to reduce the resistive loss and also antireflective coating (ARC) were introduced to further

increase the efficiency and absorb more light energy. The research in higher solar efficiencies and improved theoretical understanding provoked effort in solar cells utilizing materials other than silicon like Gallium Arsenide(GaAs), Indium Phosphide(InP), Cadmium Teleride(CdTe), Cadmium Sulfide(CdS). Despite the development in different materials for solar cell till date most of the significant solar cells uses Silicon devices.[2]

<u>1.2 Photovoltaic Cost, Market and Forecasts</u>

1.2.1 Photovoltaic Cost and limitations

The sources of which are available to mankind on earth are divided into two categories that is (1) renewable and (2) non-renewable energy sources. Among the non-renewable energy are fossil fuels (coal, oil and gas), Geothermal, Nuclear Fission and Nuclear Fusion and renewable energy being the Hydropower(dams and tides), Wind Energy and Solar Energy. Since 1800 to 1990 the per capita energy use(kwh/year) rose from 12,000 to 99,600. The average annual energy consumption for each person has changed from approximately 2,930 kwh in 1850 to 24,600 kwh in 1990.The United States(U.S.) consumes roughly 20% of the world's usage. In U.S. the energy consumption in 1990 rose from 7699.5(Kilograms of oil equivalent (kgoe) per person) to 788.5 kgoe till 2005 [3],[4]. The figure 1.1 explains the distribution of the energy consumption as averaged over the U.S. Dividing the energy into comfort heat(Heating and cooling residencies, stores, factories , hot water, etc.), process heat(in manufacturing) and work(electricity, transportation, etc.)[5],[6].
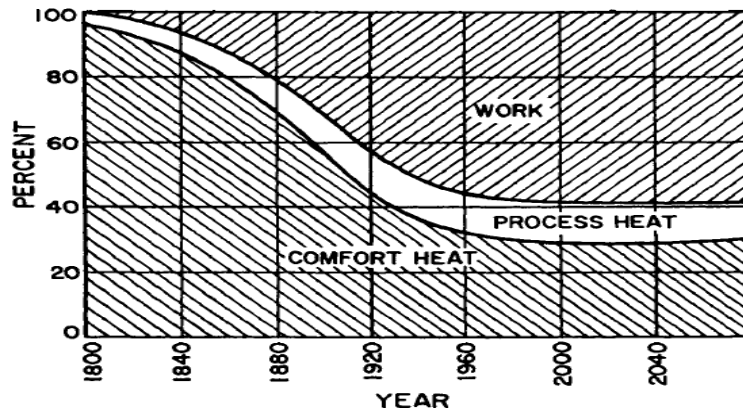
Figure 1.1 A projection of the relative proportions of three components of the energy use system, to the year 2050, for the U. S.[5]

The Primary Energy consumption(including oil, natural gas , coal, nuclear and hydro power)by U.S. from the year 1998 to 2008 has been shown in figure 1.2 and it can be seen that the energy(in million tones oil equivalent) rose from 2219.2 in 1998 to 2299 in 2008. Oil Therefore the energy consumption is bound to rise over the years and demand for energy cannot be fulfilled alone by fossil fuel or any other sources alone[7].
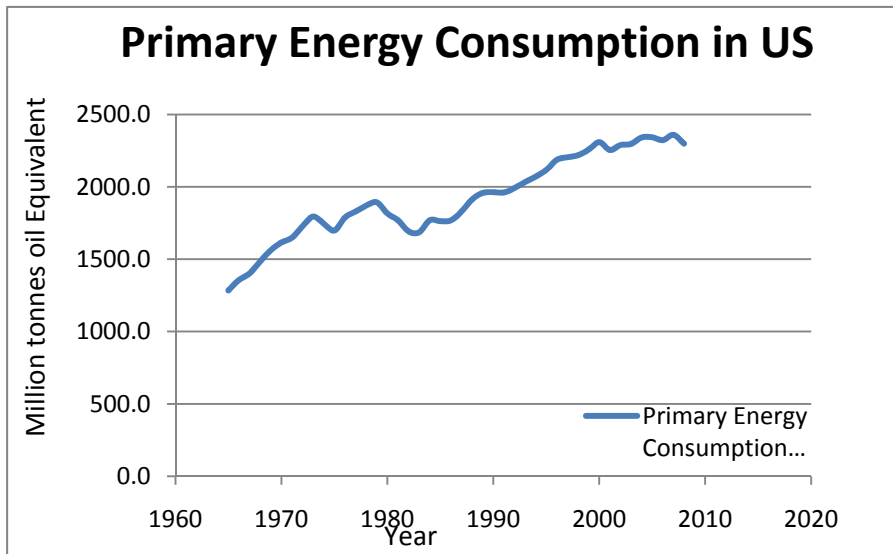
Figure1.2 Primary Energy Consumption in U.S. in millions tones equivalent.[7]

4

The need for renewable and clean source of energy is inevitable, the most abundant source of energy which is available to earth is sunlight and photovoltaic cell makes use of the sunlight to provide us with energy in the form of electricity. On an average earth receives 1.2×10^{17} W of solar energy per hour and the energy consumption worldwide at present is around 1.3×10^{13} W a year. Hence it is evident that Earth receives more energy in an hour than the total amount of energy required in a year and thus it has the capability to meet all the earth's energy need for the coming future. No other renewable energy sources has the capability to meet this requirements and therefore all other kind of renewable sources can serve as an additional source of energy in the coming future energy mix. The area required for photovoltaic cells is nominal as a typical PV module has a 10% efficiency and so having a area of 0.16% of the Earth's surface with 10% efficient solar cells would provide us with approximately 2×10^{13} W of electricity which is more than the current energy requirement of the planet. The current global PV installed capacity is around $3GW_p$. The peak watt(W_p) is the power in watts produced by a solar module when illuminated under standard conditions, standard conditions being 1,000W/m^2 intensity, temperature of 25ºC and an air mass AM 1.5(a spectrum when sunlight has passed through the atmosphere when the sun is at a 42º elevation from the horizon. Figure 1.3 shows the plot of annual PV power production vs. time for the period 1988 to 2003 [8],[9],[10].
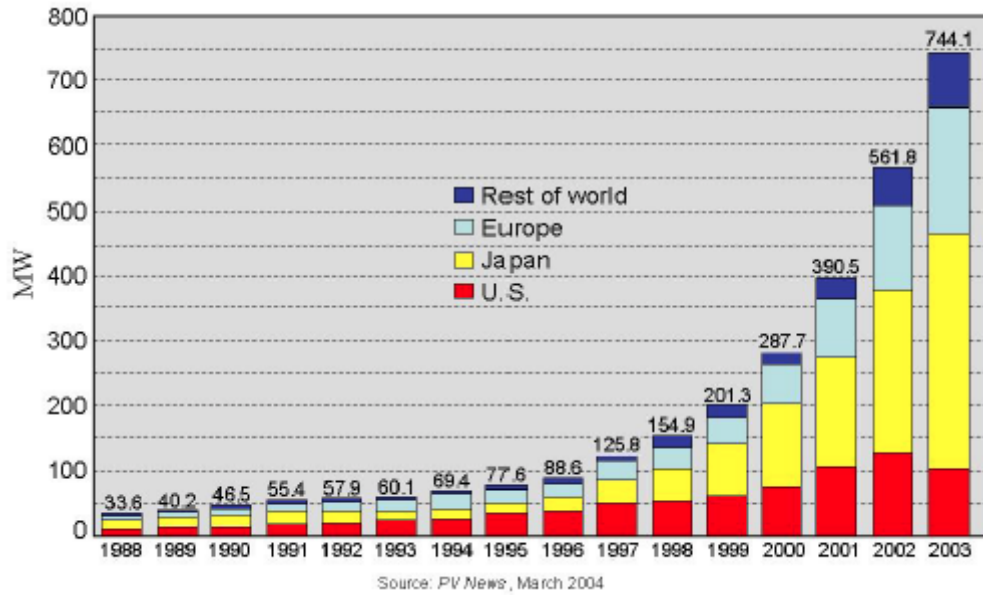
Figure 1.3 World PV cell/module production(MW_p)[10].

The cost figure of merit for PV cell modules ($/$W_p$) is the ratio of the module cost per unit area($/m^2$) to the maximum amount of electric power delivered per unit of area. In figure 1.4 the cost per peak watt is indicated.

From figure 1.4 present single-crystalline Si-PV cells with efficiency of 10% and a cost of $350/m^2$ has a module cost of $3.50/W_p$ and area I represents the first generation solar cells. In addition to module cost, a PV system also has costs associated with the non-photoactive parts(electrical installation, inverters, support structure and building integration) of the system called Balance of system(BOS) costs which are in the range of $250/m^2$ for Generation I cells and hence the total cost of present PV system is about $6/W_p$.
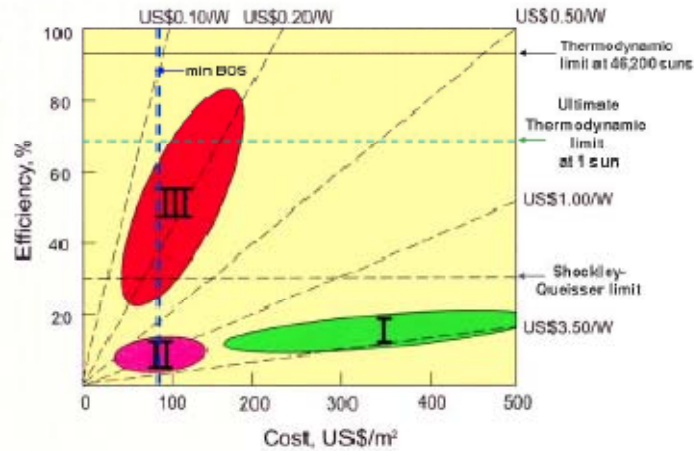
Figure 1.4 PV power costs($/W_p$) as a function of module efficiency and area cost.[8]

Areas labeled II and III in figure 1.4 gives the module cost for Generation II(thin film PV) and III(advanced Future Structures) PV cells. Following Table 1.1 gives the current and expected capacity costs of different kind of solar cells.

Table 1.1 Ranges of current and expected near term capacity costs for Four PV technologies.[11]

Capacity costs($/W_p$)	Stand-alone PV System	Grid-connected PV system.
Single Crytalline Silicon	5-30	3-8
Multi-crystalline silicon	5-30	3-8
Amorphous Silicon	4-30	2-7
Other Thin Film	4-30	2-7

For thin-film technologies, solar module cost can be expected to be around 1-3 $/W_p$, so that the total system costs lie within 2-7 $/W_p$. Present and near cost for stand alone PV systems lie in the range of 5-30 $/W_p$ for crystalline silicon and 4-30 $/W_p$ for thin film technologies. The trend in solar module price,1982- 2007 is shown in figure 1.5.
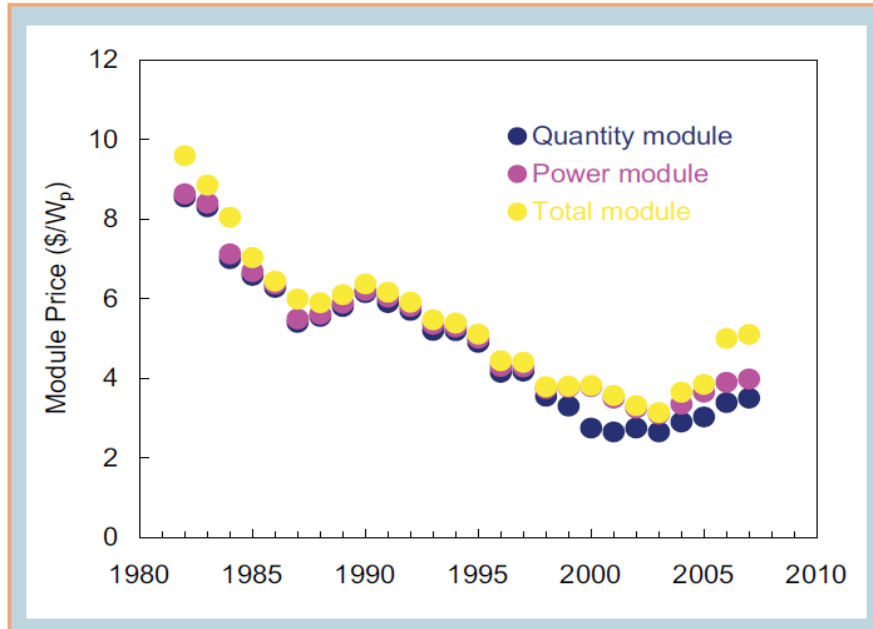
Figure 1.5. Trend in solar Module price, 1982-2007(courtesy of paula Mints, Navigant Consulting PV service Program)

The high cost wafer silicon is mainly due to the complex manufacturing cost involved. The material cost is the largest contributor to the overall cost of wafer-Si cells at ~ 50%(Figure 1.6). The industrial process for manufacturing single-crytalline Si cells is shown in figure 1.7.
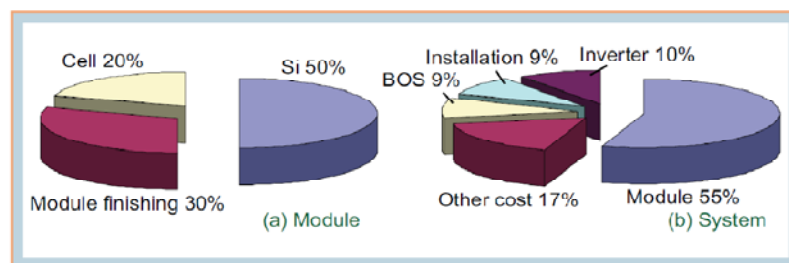
Figure 1.6 Cost Breakdown of Solar Module and systems. [10]

The metallurgical Silicon is produced from the quartz at 1900ºC and is only ~99% pure which is not suitable for solar graded silicon. The energy input for this process is 50 kWh/kg and worldwide production is ~600,000 tons/year which again releases several million tons of

8

greenhouse gases. The required impurity level for solar grade(SG) Silicon(Si) is ~ 1ppma or six

nines(99.9999%). The Metallurgical-grade Si(MG-Si) is reacted with HCl to form $SiHCL_3$ which

is purified by multiple distillation and then it is reduced by H_2 to produce high purity poly-Si. The

Temperature it requires is around 1,150ºC and an energy of ~200 KWh/Kg. Then the high purity

poly-Si is crystallized to single crystalline silicon(sc-Si) by the Czochralski process at 1,414 ºC

with an energy input of ~100kWh/kg. Then also there is an electricity consumption due to slicing

of ~700kWh/kg and a material loss of ~30%[9].
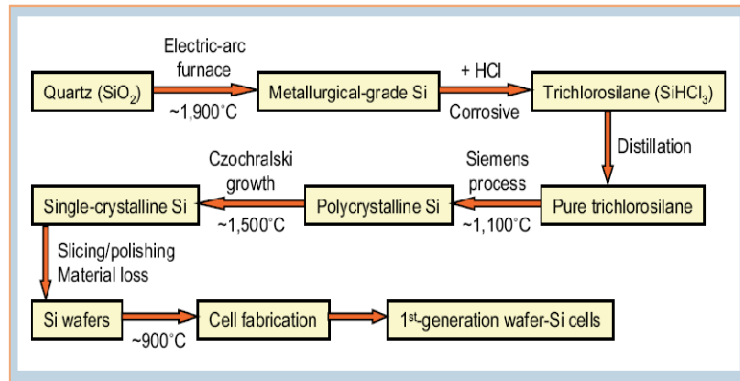
Figure 1.7 Industrial process from quartz to single crystal silicon cells.[9]

Therefore if sc-Si are to be used at $5x10^{11}$ Wp a year which can generate 4% of

worldwide electricity production in 2005, the amount of wafer required is ~2,350,000 tons/year

and this requires ~$1.6x10^{12}$ kWh or ~10%of worlds electricity production. This is the

fundamental limit to the sc-Si to make a significant contribution into the energy market. Figure

1.8 shows the production cost of electricity in US in 2002.
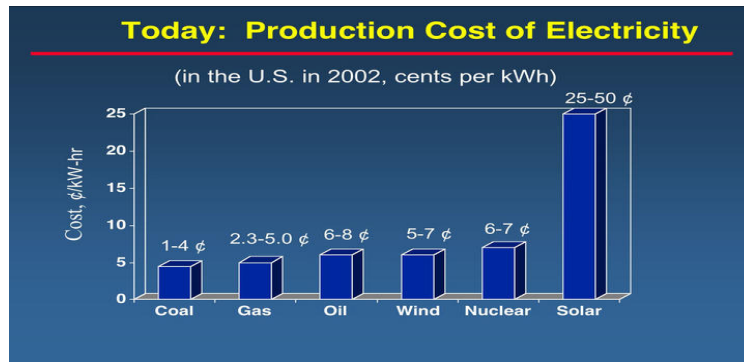
Figure 1.8 production cost of electricity.[1]

In comparison to the amount of solar energy we receive the PV accounted only 0.014% of the electricity consumed in US in 2005[10]. However worldwide the solar electricity contribution was higher due to many PV module installed in Europe and Japan, even though the number is insignificant. Assuming the demand for electricity will double by 2050 then the solar cell company will have to grow ~1000 fold in size to contribute to just 10% of the electricity we consume. Therefore there is an immense potential of solar industry and also huge gap in solar energy utilization.

1.2.2 Evolution, PV industry and future trend

Figure 1.9 shows the historical progress of the best reported solar cell efficiencies to date. The graph gives the various PV technologies of single-crystal Si, thin films, multiple-junction cells, and other emerging technologies. From figure 1.9 it can be seen that the efficiency of sc-Si cells has reached 24.7%, while that of poly-Si 20.3%. The Tandem Cells holds the record efficiency at 40.8% which is a stack of three p-n junctions made of $Ga_xIn_{1-x}As$ or $Ga_yIn_{1-y}P$ with different compositions. Besides wafer Si, thin film PV technologies has been commercialized, including Si including amorphous Si(a-Si) or microcrystalline(μc-Si) and metal chalcogenides(CdTe and $CuIn_xGa_{1-x}Se_2$(CIGS)). The laboratory efficiency has been found to be in between 12-20% but commercially sized modules are typically one-half to two-thirds of these efficiencies.

10

The present solar cell industry is dominated by silicon with ~90% of the market share. Over the last 10 years the market share of polysilicon has risen significantly compared to a-Si and sc-Si and also the market share of CIGS and CdTe is also expanding. Figure 1.10 shows the market shares of different PV technologies. The dominance of Si in the present solar market is due to the semiconductor industry which developed by the late 1950s and by the 70s material science, device physics and fabrication technology had been established and researched. However the economy of solar industry is very different from the IC industry. The basic difference is the Moore's Law which does not apply to the solar industry as because to get more energy we require more solar cells.
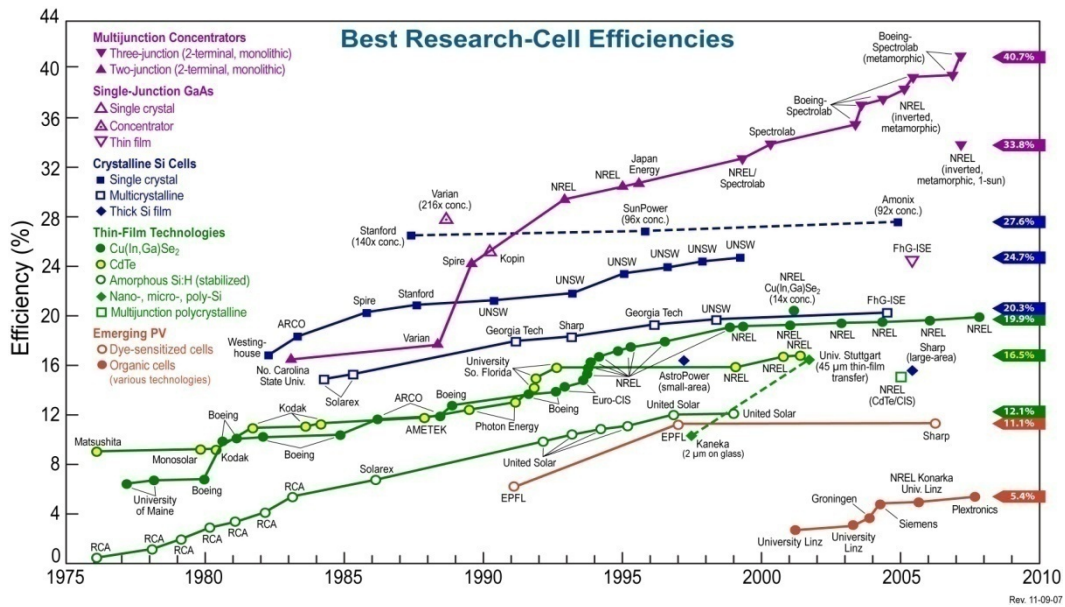
Figure 1.9 Evolution of best laboratory efficiency for different PV technologies.[1]

Over the past decades solar industry relied on production scale up and process improvement and hence the result is more or less linear growth in comparison to the exponential growth of IC industry.

11
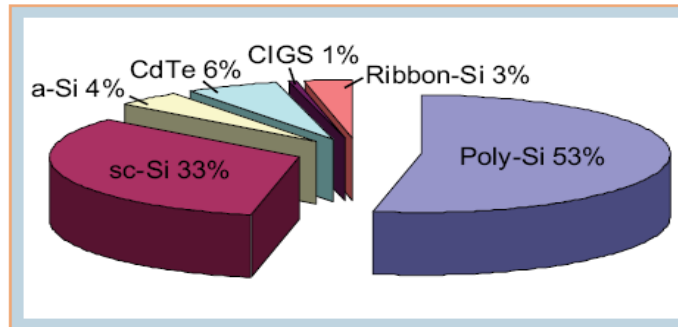
Figure 1.10 Market share of different solar cell technologies in 2007[9]

The solar PV market exhibited a global growth rate of more than 40 percent per annum over the last decade though it faces two fundamental challenges production cost and growth of production capacity.

Many semiconductor industry is using the knowledge of the IC industry to research more into Silicon based solar cell, for example, the Belgium based research institute is using proficiency from advanced deep sub micron technology to use in thin film PV cells. Even Chip equipment manufacturers are also using their experience to get a entry into the solar market. However as more industries invest in solar market and while it grows as a mass production market the development and deployment of industry standards is critical. According to Gartner reports for its Forecast of the PV solar cell market, PV market will grow at 17%CAGR(compound annual growth rate) between 2008 and 2013 to reach $34 billion revenue by 2013. Gartner estimated that after years of double digit growth the worldwide PV market reached a $16 billion mark in 2008 and forecasted that markets revenue will decrease 1% in 2009 but on GW(gigawatt) basis the overall PV market will grow 24% in 2009. Despite the rapid growth of thin-film PV the crystalline Si will remain the dominant PV technology in the market. The development of clean energy technology is going to be the key in the future growth of the major industrialized economy. Figure 1.11 shows the PV market estimates worldwide [12][13][14].
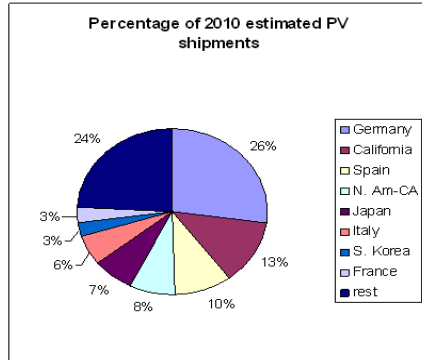
Figure 1.11 Photon International 2010 PV market Estimates.[1]

The limit to the exponential growth of PV industry is due to the lack of a optimum semiconductor. The present cells needs to be deployed on a scale of 10^{12}W to have a significant impact in the energy mix. The desired properties of semiconductors in the solar cells has been listed in Table 1.2, which shows the trade-offs between different semiconductor material for solar cell and no semiconductor material meets all the requirements. Silicon seems to be have a band gap of 1.1eV and the optimum bandgap for solar cell is 1.4eV. However due to advanced technology and research in the silicon, the crystalline silicon holds the larger share of the market share in the PV industry [9][11][12].

Table 1.2 Material requirements for terrestrial solar cells. [9]

Material Requirement	Material Meeting Requirement
1. Abundant material	Si
2. Low-cost material	CdTe, CIGS
3. Low-cost synthesis	CdTe, CIGS
4. Non-toxic material	Si, CIGS
5. Stable material	Si, III-V, CdTe, CIGS
6. High mobility	Si, III-V, CdTe, CIGS
7. High carrier lifetime	Si, III-V
8. Suitable band gap	III-V, CdTe, CIGS
9. Control of conduction type	Si, III-V, CdTe, CIGS
10. Control of resistivity	Si, III-V, CdTe, CIGS

To reduce the cost of silicon wafer, approaches like the amount of Si material used in solar cells which can be achieved by reducing the thickness of the wafer and reducing the

13

material loss during ingot slicing. It is expected that the wafer thickness in next 10 years will reduce to 100μm or less from 200μm. in addition new materials may replace Si solar cells for example in the case of CdTe or CIGS, even though they require low energy input to manufacture and their market share is increasing but the downfall is that Tellurium is scarce and cannot meet 10^{12}W demand. Hence there are always tradeoffs between different solar cell materials. The key issue with the high cost is due to the fact that manufacture of Silicon which posses a covalent bond which makes it very tough to slice the wafer and also is very energy intensive and also require a high temperature process as described figure 1.7 above. Hence it would be useful to use material with ionic bond(CdTe or CIGS) but we have to look for abundant material in nature. As a matter of fact solution processed CIGS cells are being commercialized with over 10% efficiency[16][17], recent development includes electrochemical deposition of CIGS[18], spray deposition of CIGS[19], electrical contacts by direct writing[20] and surface texture by solution coating[21].

It is very much evident from the present market growth and the research in the material for solar cell that photovoltaics will become an important source of electricity in the coming generation. With public support and right initiative by the government PV industry has a potential for substantial growth.

CHAPTER 2

SOLAR CELL DEVICE PHYSICS

2.1 p-n junction device physics and I-V characteristics

The solar cell resembles a p-n junction diode. Figure 2.1 shows the built-in potential and depletion layer width of an abrupt p-n junction. The built-in potential ψ_{bi} is given by equation 2.1 and the depletion layer width is given by equation 2.2. An Electric field develops due to the
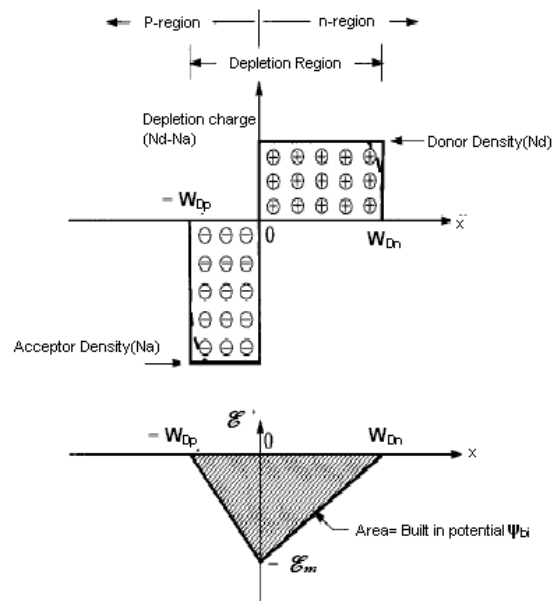
Figure 2.1 Abrupt p-n junction showing the depletion region and the built in potential.

$$\psi_{bi} = (kT/q)\ln(\frac{N_D N_A}{n_i^2})$$ 2.1

$$W_\text{D} = \sqrt{\frac{2\epsilon s\ (\psi bi - \frac{2kT}{q})}{qN}}$$

2.2

space charge region formed at the metallurgical junction between the n and p-type regions which is due to the equalization of the Fermi level E_f throughout the device, a condition of thermodynamic equilibrium; N_A doping concentration of the p-type region and N_D is the doping concentration of the n-type region. The concentration of holes and electrons can be expressed as

$$n = n_\text{i} exp(\frac{E_\text{fn} - E_\text{i}}{kT})$$

2.3

$$p = n_\text{i} exp(\frac{E_\text{i} - E_\text{fp}}{kT})$$

2.4

where n_i is the intrinsic carrier concentration and E_i is the intrinsic energy level and E_{fn} and E_{fp} are the quasi Fermi levels for electrons and holes. At equilibrium $E_{fn} = E_{fp} = E_f$, the electron and hole currents can be expressed in terms of gradients in their respective quasi-fermi levels,

$$J_\text{n} = q\mu_\text{n}n\nabla E_\text{fn}$$

2.5

$$J_\text{p} = q\mu_\text{p}n\nabla E_\text{fp}$$

2.6

where μ_n and μ_p are the mobilities of electrons and holes and in this case J_n and J_p are both zero because it is in quasi-fermi levels. Figure 2.2 shows the energy band diagram of a p-n homojunction under no bias.

16
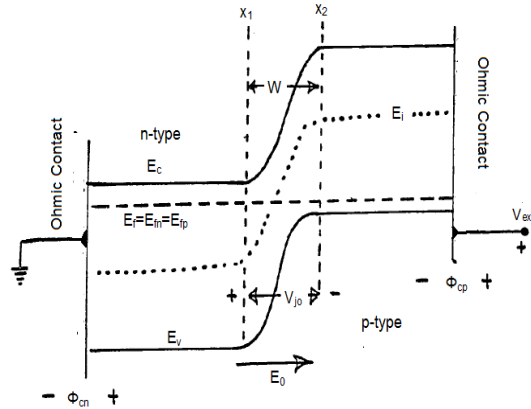
Figure 2.2 p-n homojunction under no bias.

The built-in potential is given in equation 2.1 which says that the potential barrier of the junction increases with doping and the open circuit voltage depends primarily on built in voltage. The junction under forward bias is shown in figure 2.2 and this positive voltage lowers the junction potential Vj so that,

$$Vext = \Phi cn \ + \ \Phi cp - Vj \qquad\qquad 2.7$$

where Φ_{cn} and Φ_{cp} are potentials formed at the ohmic contacts. The ohmic contact potentials remain constant and do not change appreciably under conditions of biasing, current flow and optical or thermal injections[23]. The total current due to forward bias is given by,

$$J=J_p+J_n \qquad\qquad 2.8$$

quasi-neutral, simplifies the calculation of the current. The minority carrier current diminishes away from the junction due to recombination mechanism. The current continuity is maintained by the majority carriers supplied by the ohmic contacts and therefore the minority carrier current at the edges of the depletion region still determines the total current in the device.

In the forward bias when the p-side is in positive potential relative to the n-type and in vice-versa for the reverse bias case. The diagram is shown in figure 2.3.

17
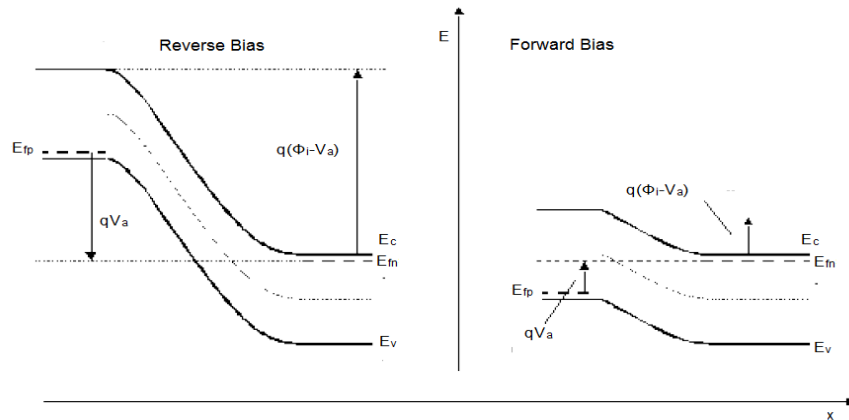
Figure 2.3 band diagram for Forward and Reverse Biased p-n junction.

The I-V characteristic of a p-n junction diode under applied voltage is shown in figure 2.4, when there is a large increase in the reverse current, the reverse bias approaches breakdown voltage, which corresponds to Emax(maximum field) approaching Ecrit. In the forward region there is a threshold region before the diode starts to conduct [23][24].
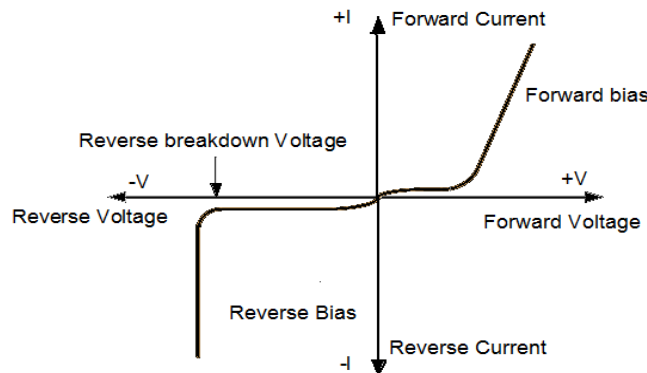
Figure 2.4 I-V characteristics of junction diode.

2.2 Solar spectrum and solar cell device operation

The energy from the sun reaches the earth in the form of Electromagnetic radiation in the ultra-violet to infrared(wavelength of 0.2µm to 3µm). In every second the total amount of

18

energy produced in the sun is 4 X 10^{20} J. The intensity of solar radiation in free space at the average distance of the earth from the sun is called the solar constant having a value of 1353W/m^2. The air mass is the degree to which atmosphere affects the sunlight received on the earth's surface and it is the secant of the angle(sec θ) between the sun and the zenith[25]. The total incident power for AM1.5 is 844 W/m^2. Solar spectrum at different air mass is shown in diagram 2.5.
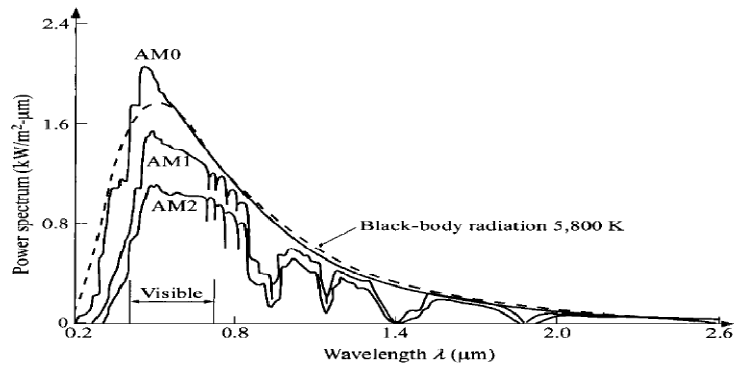
Figure 2.5.Solar Spectrum at different Air Mass.[26]

The number of photons in unit energy range per cm2/s for AM1.5 and AM1.0 is shown in figure 2.6.
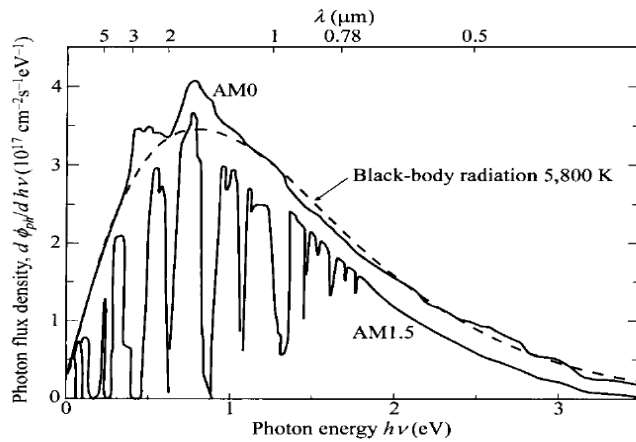
Figure 2.6 Solar Spectrum as a function of photon energy for AM0 and AM1.5 conditions.[25]

19

Figure 2.7 shows the device operation under illumination, the photogeneration excess carriers results in an external photovoltage. The external voltage or the open circuit voltage V_{oc}[27] is given by,

$$V_{ext} = V_{oc} = K_b \frac{T}{q} \ln \left[\frac{I_{ph}}{I_s} + 1 \right]$$ 2.9

Where I_s is the saturation current of the diode and I_{ph} is the photon current, K_b is the Boltzmann constant. The external voltage V_{oc}[28] of the solar cell can also be written as

$$V_{ext} = V_{oc} = - \int^{W} (E\text{-}E_0) \, dx$$ 2.10

Where E_0 is the depletion region field for the equilibrium case and E is the field under illumination and this points up that it is the reduction of the depletion region barrier by optical injection which is responsible for photovoltage.

The quasi-fermi levels are also shown in figure 2.7 which include the gradients indicating the presence of electron and hole currents. Due to illumination there will be generation of electron-hole pairs, the minority carrier generated will be swept towards n-side for electrons and p-side for holes and thereby becoming the majority carriers on these respective sides. Only these carriers contribute to the external current in a solar cell. Minority carriers are lost to surface recombination which diffuse away from the junction and therefore it is a goal to
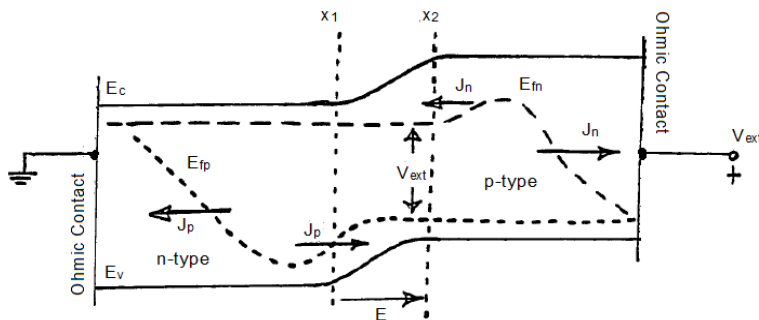
Figure 2.7 Band Diagram showing p-n junction under illumination.

20

design the cell to minimize the minority carrier surface recombination, reduction of surface carrier recombination helps to restrict minority carriers at the edges of the depletion region leading to higher excess minority carrier concentrations and hence a higher open circuit voltage V_{oc} [29].
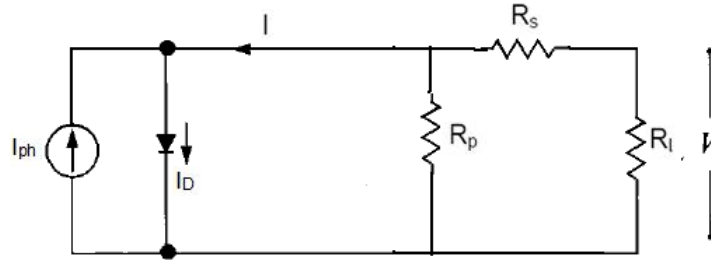
Figure 2.8 An equivalent circuit of a Solar cell.[25]

The photocurrent is directed from the n-side to the p-side and is opposed to the main diode current from the p-side to the n-side. Hence for the illuminated p-n diode, the current equation is given by,

$$I = I_D - I_{ph} \qquad\qquad 2.11$$

Where I_D is the diode current given by $I_D = Is(e^{\frac{qV}{kT}} - 1)$, and I_s is the saturation current. Figure 2.8 shows the equivalent circuit model for solar cell and figure 2.9 the typical I-V characteristics.
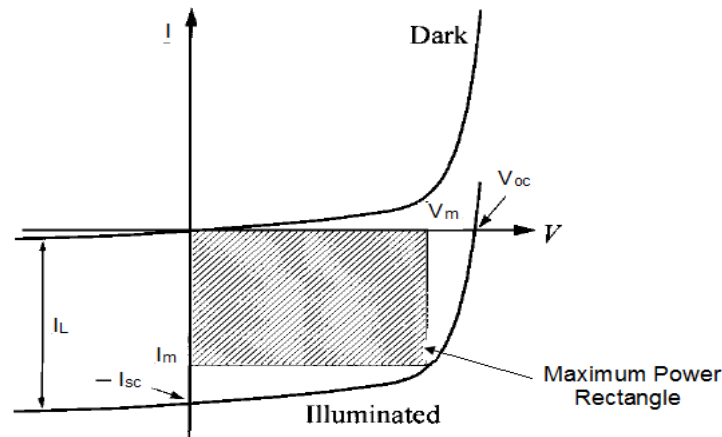
Figure 2.9 I-V characteristics of p-n junction solar cell in dark and when illuminated.[25]

The parallel or shunt resistance does not have appreciable effect on the output power of the device but the series resistance, R_s, which depends on the impurity concentration of n-type and p-type regions, and Ohmic contacts arrangements has a considerable effect on the output power. The Fill Factor is defined as ration of actual power to the theoretical power or the power extraction capacity of a solar cells, it is a performance parameter for solar cells.

$$FF = \frac{I_m V_m}{I_L V_{oc}}$$
2.12

Another solar cell performance parameter is the conversion efficiency, η,

$$\eta = \frac{I_m V_m}{P_{in}}$$
2.13

An individual silicon solar cell with an area of 2cm^2 can have an open circuit voltage of 0.5-0.6 Volts and about 20 to 60 mA of short-circuit current, solar cells are usually connected to in series and in parallel to form arrays and higher voltage and higher current can be delivered. A chart of Loss mechanism in solar cell is shown below,
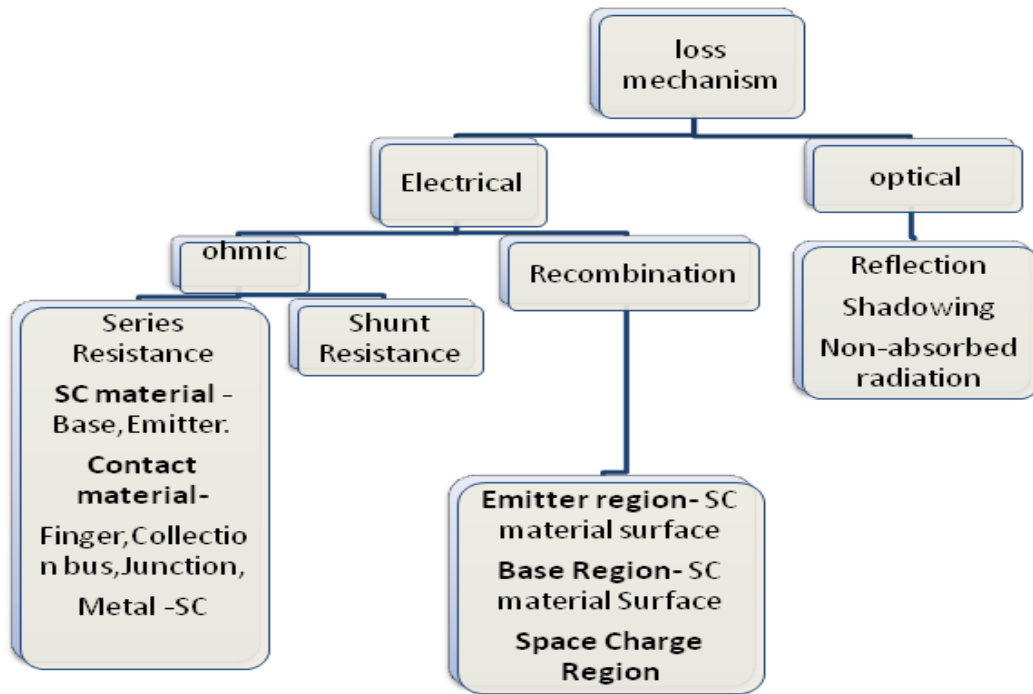
Figure 2.10 Loss mechanisms in a solar cell

2.3 Objective of this Research

The effect of light-scattering on amorphous, microcrystalline superstate thin film and polycrystalline Silicon(poly- Si) solar cell has been well studied. Unlike the single crystal silicon solar cell where the pyramids and grooves are employed which are 10μm and the structure has considerable thickness(several   100 microns) but in thin film this technique will lead to the formation of penetration through substrate and therefore this methodology cannot be used in the thin film technology and also in poly-Si at present there is no cost effective method for surface texturing to minimize reflection. In thin film solar cells the light scattering is introduced by surface roughness of the Transparent Conductive Oxide (TCO) which increases the optical path length and thereby the efficiency of the cell. The surface roughness can be introduced by depositing the Si thin film on a textured surface[31]. The TCO materials typically used are

SnO2, ITO or ZnO grown by Chemical Vapor Deposition(CVD). One other promising method of producing textured ZnO is by depositing zinc oxide by sputtering and then chemically etching it in diluted acid [32]. A much cost effective and efficient way is by electrodeposited Ga-doped ZnO layer having high transmittance ~80%, absorbance below 10% and low resistance of 3.8 X 10^{-4} Ω-cm meets the requirement of TCOs [33]. The choice of ZnO as TCO over other competitor like tin oxide or Indium Tin Oxide(ITO) is because it offers significant low cost relative to indium based systems and also it possess high chemical and thermal stability.

In this research a cost effective approach is taken to produce zinc oxide pyramidal shape micro particles which can be used as an antireflective coating on solar cell. The main goal of this thesis is developing textured(pyramidal shaped) zinc oxide particles for anti-reflective coating on solar cells. The idea is to form a mold out of silicon and the trick is to deposit the ZnO selectively into the molds and the approach taken to successfully deposit ZnO into the silicon mold and thus form particles is as follows: 1) A new method to develop textured zinc oxide will be described. 2) Fabrication process to develop mold in Silicon for the deposition of zinc oxide, 3) deposition of zinc oxide on ITO and silicon using electrochemical method, 4) Characterization of zinc oxide film using XRD(X-Ray diffraction), 5) extraction of parameters like reflection, transmission and absorption and bandgap calculation will be described with respect to zinc oxide deposited on ITO at different annealing temperature, 6) extraction of the particles from the silicon mold.

In the following the chapters at first the fabrication process which involves the process of deposition of silicon nitride as the hard mask for wet etching of silicon and also electrochemical deposition of the zinc oxide will be described and then the characterization techniques and results from spectrophotometry, XRD and SEM image results is shown in the next chapter.

CHAPTER 3

FABRICATION PROCESS

3.1 Anti-Reflection Coatings

The introduction of surface texturing on solar cell did not come earlier than 1954. However, the breakthrough was in 1960 when Dale and Rudenberg [35, 36] introduced the potential of surface structure for reflection control to the PV community and also presented the idea of anisotropic etching. A major issue in increasing the efficiency of solar cell device is to efficiently couple the external light into the device and antireflective coatings are developed to increase the front surface transmission.

The theory behind the antireflection coatings on high refractive index substrate like silicon is well known. A single layer anti-reflection coating has the following properties:

$$n_1 = \sqrt{n_0 . n_2} \qquad\qquad 3.1$$

$$d = \frac{\lambda}{4n_1} \qquad\qquad 3.2$$

Where n is index of refraction, d is the thickness of the film, and the λ is the wavelength of the film being designed.
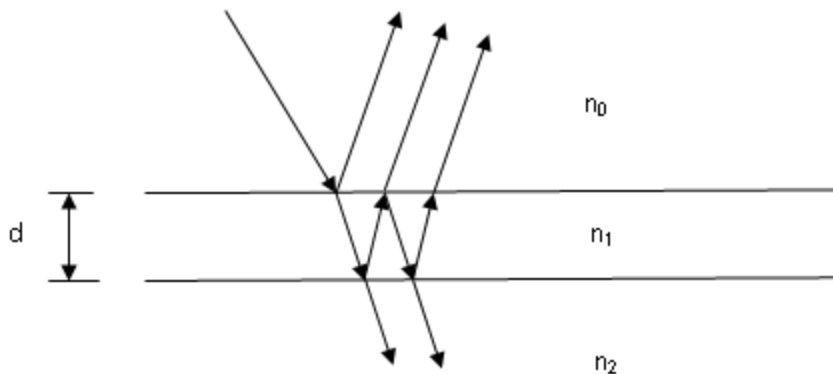

Figure 3.1.Antireflection in a thin layer.

25

For the layer thickness of d, the reflection R depends on the refractive index of all these three layers,

$$R = \frac{(n_1 - n_0 n_2)^2}{(n_1{}^2 + n_0 n_2)}$$ 3.3

Therefore the top surface in a solar cell has two important requirements. At first it should help in coupling as much light as possible and also the front surface should reflect light internally to allow the total internal reflection to occur.

The total reflection can also be reduced significantly if the surface is textured in pyramidal structure as shown in figure 3.2(a), in macroscopic features where the groove size is assumed to be large compared to the wavelength of light to employ ray tracing method to study reflection. For light incident perpendicularly to the plane of the cell, there are few threshold values of α which changes reflection on the textured surface, α (figure 3.2 (a)) greater than 30° will experience double bounce effect and by 60° all the rays experience triple bounce. Mathematically for angle $54° \leq \alpha \leq 60°$, the fraction of perpendicularly incident light experiencing triple bounces, f_3 can be related as,

$$f_3 = \frac{\sin(5\alpha - 270)}{\sin(90 - \alpha)}$$ 3.4[37]

For surface features formed by intersecting (111) crystallographic planes in silicon is 54.7° here all perpendicularly incident light will get atleast a double bounce with 11.1% incident near the bottom of the groove experiencing triple bounce.[37]

The reflection is at the same angle, so the reflected part of the light meets the opposite surface and again a part penetrates the crystal. It has been seen that randomizing(lambertian) case of pyramids is more favorable than the regular arrangement in boosting the short circuit current [37]. Both principles, surface texturing and antireflection coating can be combined to reduce the surface reflection and increase the cell efficiency. Figure 3.2(b) shows the ray path for light perpendicular incident upon groove with (111) planes and having a glass encapsulation.

26

For unpolarized light at 600nm free space wavelength, 96% of the light energy will be coupled into the glass(T1), 25.3% will be reflected after first striking the groove(T1R2) and reducing to 5.1% strongly polarized after the second groove reflection(T1R2R3) and only 3.6% couples out of the glass(T1R2R3T4). A fraction of 11.1% of incident light energy strikes the area near the base and has an additional reflection with the result of triple bounce with a 4% coupled out that is a total of 7.6% of the total incident energy is reflected.[37].
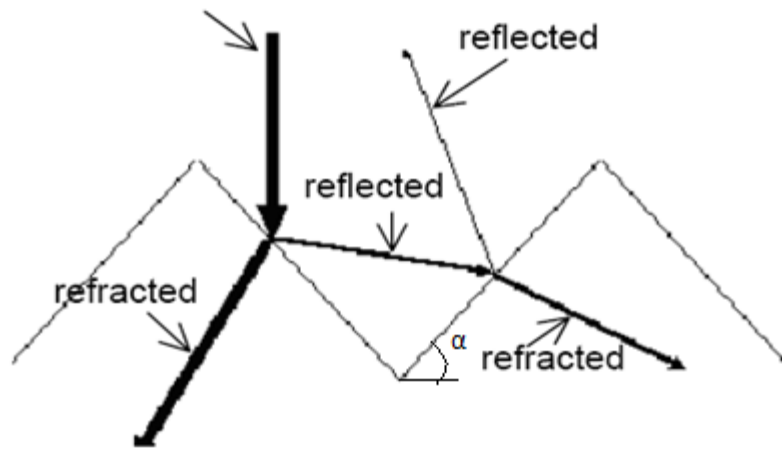
(a)
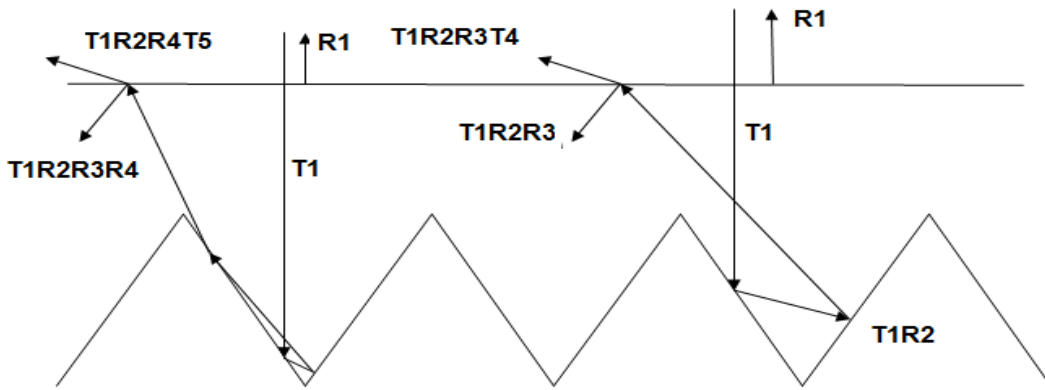
(b)

Figure 3.2(a) Reflection on the textured surface (b) Ray paths for grooves formed by intersecting(111) equivalent planes[35].

It has been also proved using simulation based on rigorous coupled-wave analysis [34] that loose packed pyramid structure has least reflectivity compared to cone-shaped or hemisphere- shaped particles. The objective here is to achieve pyramidal shaped zinc oxide which can act as antireflective coating and random pyramid for enhanced light trapping in solar cell. In the following sections the fabrication process is explained.

3.2 Fabrication Process

3.2.1. Plasma Enhanced Chemical Vapor Deposition(PECVD) of Silicon Nitride

The fabrication process involved in making the zinc oxide particles has been shown step-wise in figure 3.3. A p-type(100) wafer silicon with low resistivity 0.001-0.005 ohm-cm and thickness 500-550 μm was chosen for the process. A plasma enhanced chemical vapor deposited (PECVD) silicon nitride was used as the hard mask. The LPCVD(low pressure chemical vapor deposition) or sputtered silicon nitride could not be used as the hard mask for the wet etching as because of its resistance to most chemicals and makes it difficult for wet etching. The PECVD silicon nitride which is represented by $Si_xN_yH_z$, having the hydrogen greatly affects the etch rate

28

silicon wafer

silicon nitride,

patterned silicon nitride,

etched inverted pyramid,

electrochemically deposited
Zinc Oxide

Extracting Zinc oxide
from the silicon mold
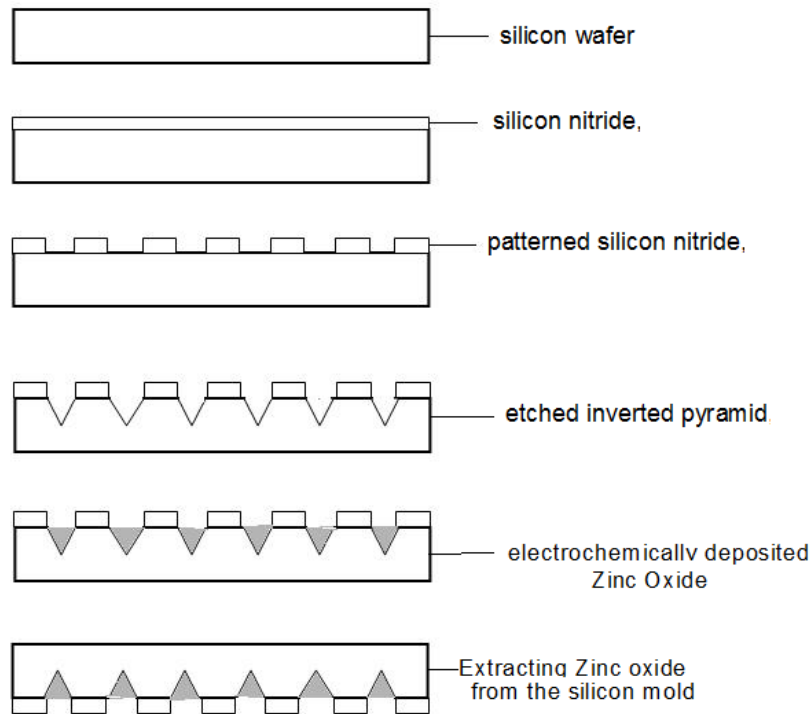
Figure 3.3 Process steps for preparing Zinc Oxide particles.

condition in buffered hydrogen Fluoride(BHF) [38]. The etch rate increases with increasing hydrogen(H) content and decreasing Silicon(Si) content. The H incorporation increases with increasing ammonia(NH3) flow and decreasing nitrogen(N2) flow and also the increase in temperature decreases the H content and also the refractive index increases with increasing Silicon content and decreasing H content [38].

The schematic diagram of the Orion III PECVD process chamber is shown in figure 3.4 below, the process chamber is made up of vacuum enclosure having the inductively coupled plasma(ICP), the chamber block and the reactive ion etch(RIE) matching network.

Figure 3.4 Overall Process Chamber with ICP [40]

During a process, the process gases enter at the rear of the ICP, flow through the center of the ICP lid and exit into the chamber volume at the top center. A mass flow controller controls the gas flow to the chamber. The helium gas can also be introduced into the chamber through the chuc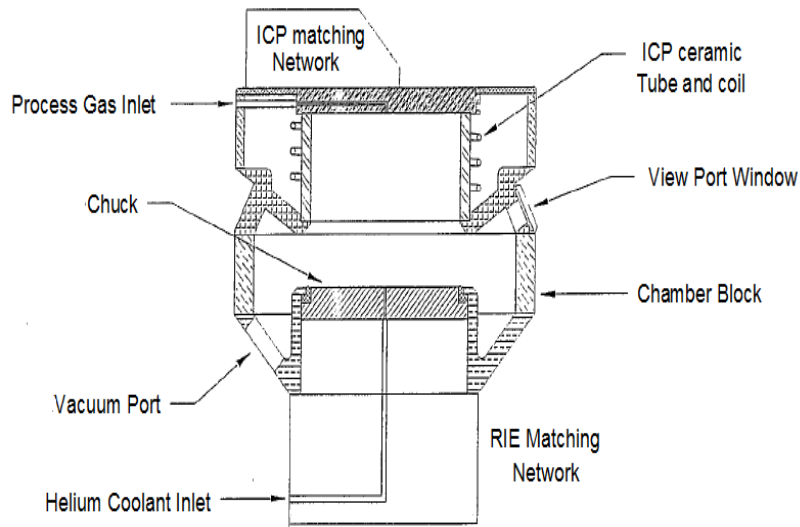k which helps to cool the sample. The gases are sucked out of the chamber through the vacuum port at the rear of the chamber. The plasma is created when the RF generators for the RIE and the ICP are turned on. The sample is loaded into the chamber by the help of the load lock chamber which is connected to the process chamber via a gate valve. With the help of the robot arm the sample is transferred to the process chamber, but before opening the valve the load lock pumps down the pressure to 100mTorr. There are two RF generators one for the ICP and another for the RIE source which are of 3000Watt and at 13.56 MHz.

The silicon nitride was deposited at a pressure of 500mTorr and the flow rate of Ammonia(NH_3), nitrogen(N_2) and the ratio of Silane to Argon (SiH_4/Ar) was kept at 50sccm (standard cubic centimeter per minute), 250 sccm and 20 sccm respectively. The deposition rate was found to be 5 Å/second and the deposited film thickness was 250-300 nm(nanometer).

The deposited silicon nitride was then annealed in N_2 atmosphere at 600C for 30 minutes. The annealing of silicon nitride film helps in removing the crystalline defects.

3.2.2 Patterning of silicon nitride(Si_3N_4) and inverted pyramid on silicon

A photomask having 20X20 micron square with 80 micrometer distance between each square is used. The photolithography process is carried out by KarlSuss MJB3 Mask Alligner.The positive photoresist Microposit Shipley 1813 is used to pattern the silicon nitride. The resist is spun with 4000 rpm and for 40 second to get a coating thickness of more than 1μm and then the sample was post baked for 1 minute at 90ºC to 100ºC. The coated wafer is exposed to i-line ultra violet light for 13 second totaling to energy of approximately 65mJ/cm^2 exposure and the exposed wafer is developed in MF-320 developer for 15 second. The patterned silicon nitride with photoresist is shown below in figure 3.5.
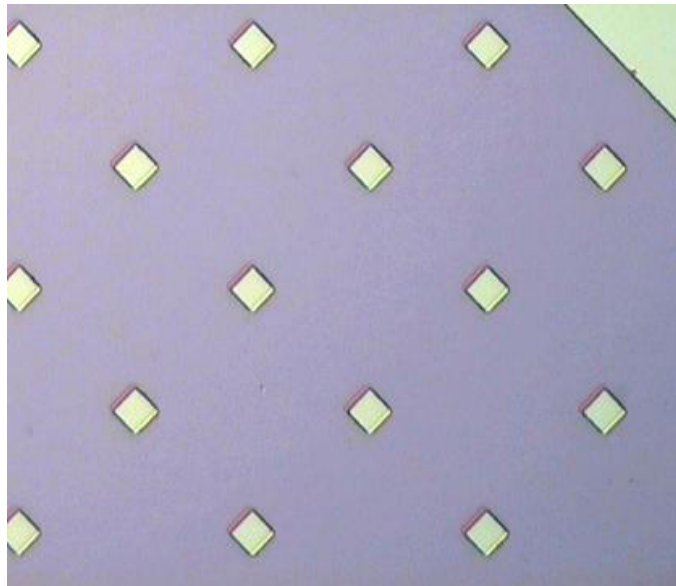

Figure 3.5 Patterned silicon nitride.

The exposed silicon nitride is then etched in Buffered Oxide Etch solution and the etch rate is found to be approximately 8.5Å/second and the photoresist is stripped of the sample by

cleaning it in Acetone and now the silicon is exposed and the silicon nitride mask is successfully created for the anisotropic etch of Silicon.

3.2.3 Anisotropic Etching of Silicon using Si_3N_4 as Hard Mask

Silicon has a diamond crystal cubic structure and the crystallographic directions are perpendicular to crystal planes. The important parameter in orientation dependent etching of silicon is the atomic lattice packing density and available bonds in the crystalographic plane. The <111> direction has a very high atomic packing density in the (111) plane. The <100> direction is 54.75º from the <111> direction and <110> direction is 90º from the original <111> direction. The atomic density in these planes is lower compared to {111} plane. Hence it is evident that the etch rate is faster in <110> direction than in the <100> direction and even more than <111> direction. The {111} and {100} planes are perpendicular to each other and they intersect at 54.74º angle and that they are in <110> direction [41]

The silicon nitride masked p-type {100} silicon wafers are alligned parallel or perpendicular to <110> directions. The patterned wafer is placed in a direction oriented wet etchant consisting a mixture of potassium hydroxide(KOH) and isopropyl alcohol(IPA) and water(H_2O) having 23.4 wt% KOH, 13.3 wt% IPA and 63 wt% water. The etch rate for this etchant is 100 times faster in (100) plane to (111) plane. The wet etching is carried out at a temperature of 80ºC in hot water bath for less variation in the temperature. The etching rate is found to be 0.5µm/minute along (100) plane and 0.006 µm/minute along (111) planes. The etching pattern profile is shown below in figure 3.6.
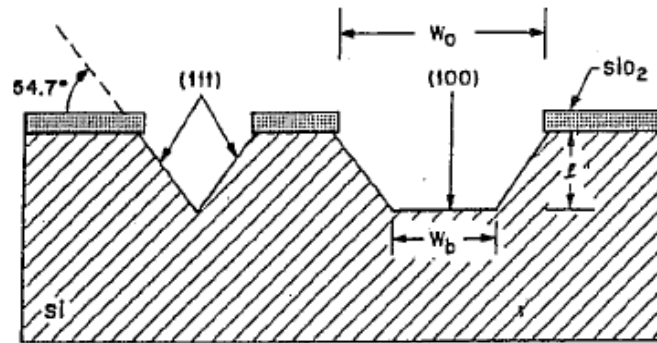
Figure 3.6 etch profile on <100> Si.[42]

This orientation etch creates a V-shaped grooves with square base as shown in the figure 3.6.

Figure 3.7 shows the SEM image of the inverted pyramids or inverted pyramid mold.
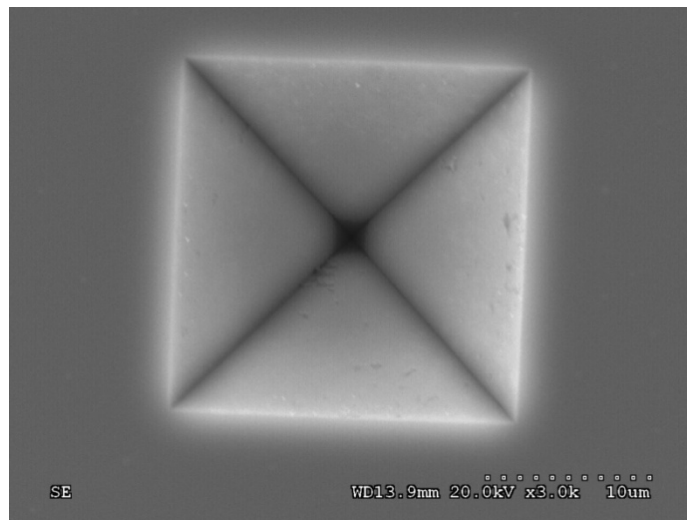
Figure 3.7 SEM image of the inverted silicon Pyramid mold.

3.2.4 Electrochemical deposition of Zinc Oxide (ZnO) on the inverted pyramid mold

3.2.4.1 Electrochemical Deposition Method

The deposition of ZnO can also be done with other deposition technique such as sputtering and chemical vapor deposition (CVD), in comparison to these deposition method electrochemical deposition method has the advantage of low cost, low temperature and ease of controlling parameters and large area deposition.

33

A electrochemical cell consists of two independent half reactions. The matter of interest is only one half reaction in working electrode(WE) and the potential of the WE is measured with respect to reference electrode(RE). The potential of the RE is fixed. Figure 3.8(a) and 3.8(b) shows the oxidation and reduction by applied potential. When a negative potential is applied the potential of WE is increased and at a particular potential the electron will transfer to the vacant state of the species in the solution. This causes the reduction of the species in the solution at the surface of WE by flow of electrons from the WE to the solution and forms the cathodic current. When a positive potential is applied the energy of electrons on the WE will be lowered and at certain potential the electron will flow from solution to WE and forms the anodic current. The critical potential which the reaction occurs is called the standard electrode potential (E^0). An electrode reaction includes four steps:

1. Mass transfer (species transferred to electrode surface)
2. Electron Transfer at the electrode surface
3. Chemical reactions preceding or follow the electron transfer.
4. Other surface reaction-desorption or adsorption.

A counter electrode(CE) is placed in the cell and current flows between WE and CE[43].

Cyclic Voltammtery (CV) is an effective and versatile electroanalytical technique available for the mechanistic study of redox system. It is the first experiment done before studying the electranalysis of an experiment. It rapidly locates the redox potentials of the elctroactive species. A typical cyclic voltammogram recorded for a reversible single electrode transfer reaction for a single electrochemical reactant is shown below in figure 3.8. In the forward sweep the voltage is swept from V1, the equilibrium at the surface begins to alter and
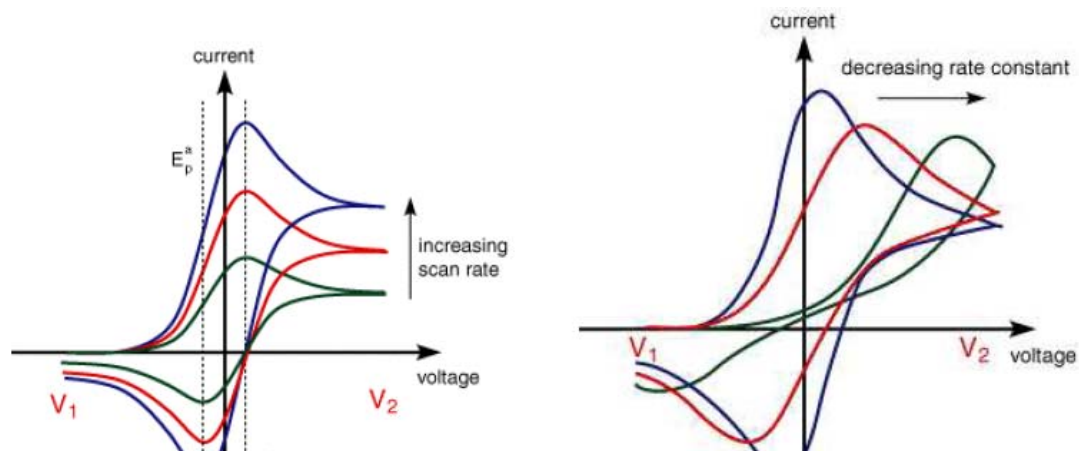
Figure 3.8 Scan rate and rate constant dependence on the I-V curve.

the current begins to flow. The current rises as the voltage is swept further from initial value as the equilibrium position is shifted further to the right hand side, converting more reactants. The peak can be seen at some point when diffusion layer has grown sufficiently above the electrode so that flux of the reactant to the electrode is not fast enough to satisfy that required by the Nernst equation. When the scan is reversed it moves back thorough the equilibrium positions gradually converting electrolysis product to reactant. The current flows from solution species back to the electrode which is in opposite sense of the forward sweep. The Nernst Equation(half cell reaction) is shown below as,

$$E_{red} = E_{red}^{\circ} + \frac{RT}{nF} \ln \left(\frac{[oxidation]}{[reduction]} \right) \qquad 3.4$$

Where E_{red} is the half cell reduction potential, E_{red} is the standard half-cell reduction potential, R is the universal gas constant: R= 8.314 JK^{-1} mol^{-1}, T is the absolute temperature, F is the faraday constant F= 9.648 X 10^4 C mol^{-1}, n number of electrons transferred in the half-cell reaction.

3.2.4.2 Electrochemical Deposition of Zinc Oxide

The cyclic voltammetry(CV) is performed on a solution containing 0.1M $Zn(NO_3)_3$[44] at 60°C with WE as the p-type (100) silicon with resistivity of 0.001-0.005 Ω-cm and metallic zinc as the CE, the deposition temperature was controlled by Precision 280 water bath to 60°C, the figure 3.9 shows the CV curve, which showed two reduction reactions,

$$NO_3^- + H_2O + 2e^- \rightarrow NO_2^- + 2OH^- \qquad\qquad 3.5$$

$$Zn^{2+} + 2e^- \rightarrow Zn \qquad\qquad 3.6$$

The deposition was carried at -1.2V. The produced OH- ions react with Zn^{2+} ions in the solution to form ZnO:

$$Zn^{2+} + 2OH^- \longrightarrow ZnO + H_2O \qquad\qquad 3.7$$

The current was in the range of 5-12mA for one hour deposition. The deposition rate was 0.7μm/minute.

The deposition was also carried out on ITO coated glass which was prepared using AJA ATC ORION Series UHV Sputtering System. The ITO film had a resistivity of 0.5 X 10^{-3} Ω-cm and the deposition rate of ZnO on ITO was 1.7μm/hr.

The images are taken using ZEISS Supra 55 VP Scanning Electron Microscope(SEM) and it is shown in figure 3.10 and figure 3.11. In figure 3.10 we can see that some inverted pyramids. The deposition of $Zn(NO_3)_3$ is also done on ITO which is deposited on a glass slide using sputtering and the cyclic voltammetry measurement is done on 0.1M $Zn(NO_3)_3$ and platinum electrode as the counter electrode and ITO coated glass as the working electrode and the deposition is done at 0.4V and the thickness obtained is ~2μm. The cyclic Voltammetry curve is shown in figure 3.10.
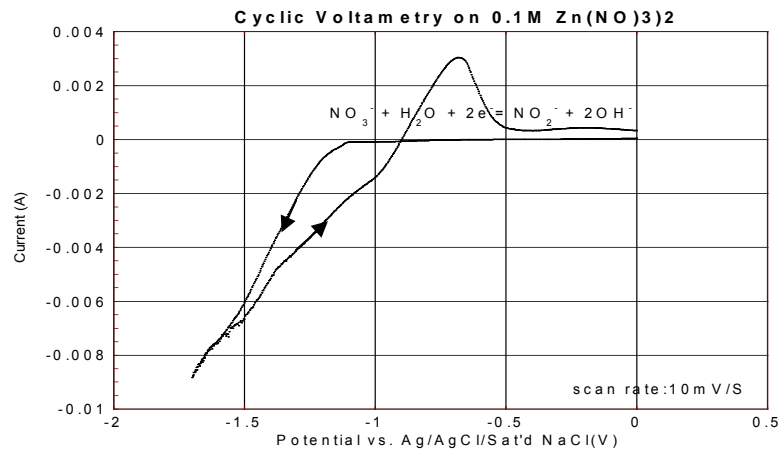
Figure 3.9 Cyclic Voltammtery of a deposition solution containing 0.1M $Zn(NO_3)_3$ at 60ºC
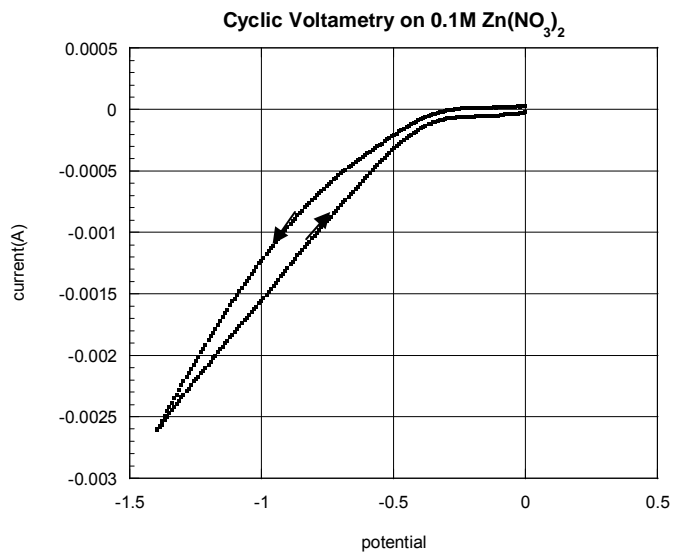

Figure 3.10 Cyclic Voltammetry on ITO coated glass having solution containing Zn(NO3)2 at 70 ºC
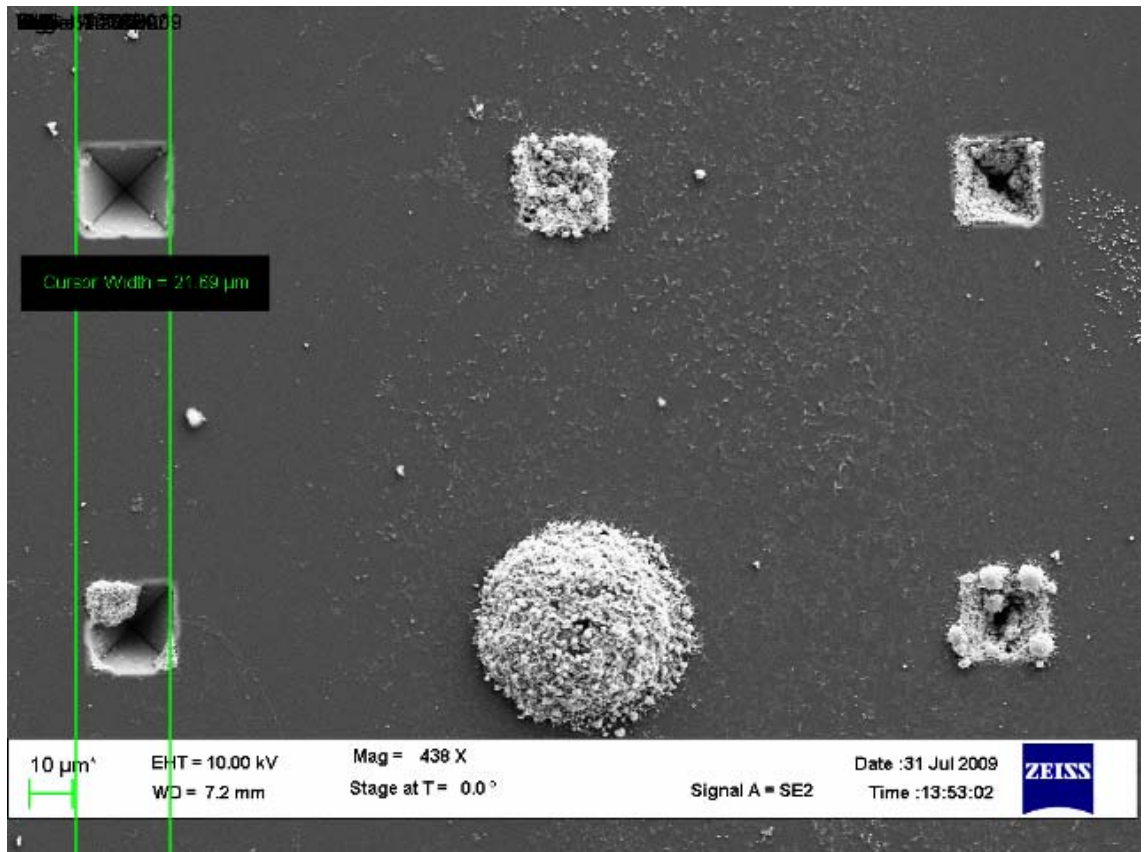
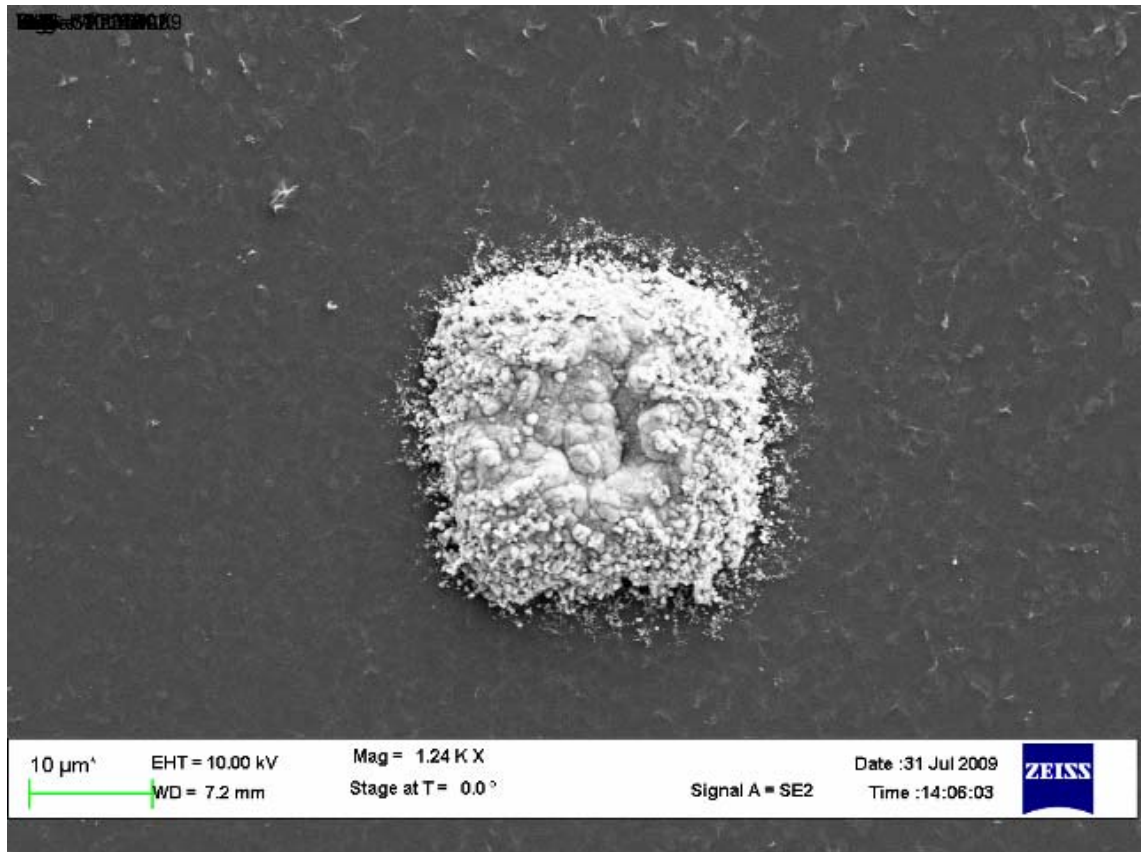Figure 3.11 ZnO deposited on etched inverted pyramid.

Figure 3.12 Zinc Oxide deposited completely inside the pyramid.

In the following chapter the optical characterization, bandgap calculation, X-ray Diffraction including the SEM images of the particles are shown.

CHAPTER 4

CHARACTERIZATION AND RESULTS

The deposited zinc oxide using the electrochemical deposition method as described in the section 3.2.4. is characterized for its thickness, crystal orientation, optical properties and bandgap of the deposited zinc oxide is calculated from the results.

Zinc oxide has a wurtzite structure, shown in figure 4.1, and has a hexagonal lattice and is characterized by two interconnecting sublattices of Zn^{2+} and O^{2-} in such a way that each zinc ion is surrounded by a tetrahedral of O^{2-} ions, and vice-versa. The tetrahedral coordination indicates a covalent bonding, however it also possesses very strong ionic character and hence zinc oxide is considered to lie on the borderline between covalent and ionic compound class. The lattice parameters of the hexagonal unit cell are a=3.2495Å and c=5.2069Å and the density is 5.605 gm/cm3. The energy band gap of zinc oxide is found to be 3.4eV and the valence band maxima and conduction band minima occurs at k=0 indicating it is a direct band gap material [43].

In the following sections all the characterization technique such as spectrophotometry, XRD involved in the research are explained with the result.

4.1 X-Ray Diffraction(XRD)

4.1.1 Principle and Operation

The interaction of X-rays with crystalline matter is its diffraction, produced by the reticular planes that form the atoms of the crystal. A crystal diffracts a X-ray beam passing through it to produce beams at specific angles depending on the x-ray wavelength.

According to Bragg law, the incident, the normal to the reflecting plane, and the diffracted beam are always coplanar; the angle between the diffracted and the transmitted beam is always 2θ. These condition is described by the Bragg law:

$$2d\ sin\theta = n\lambda$$ 4.1

where n is an integer, λ is the wavelength of the radiation and d is the spacing between surfaces and θ is the angle between the radiation and surfaces. This relation illustrates that interference effects are observable only when radiation interacts with physical dimensions that are approximately the same size as the wavelength of the radiation.

A x-ray diffractometer consists in an X-ray generator, a goniometer and sample holder and an x-ray detector, such as photographic film or a movable proportional counter. The most commonly used instrument for generating x-rays are x-ray tube, which generates x-rays by bombarding a metal target with high energy(10-100keV) electrons. Two common targets are Mo and Cu which have K_α x-ray emissions at 0.71073Å and 1.5418Å. In powder diffractometers a photon detector is replaced by photographic film or annular detector[46].

The rays diffracted by the specimen at an angle 2θ which converge to a line at the receiving slit and the x-rays are detected by a radiation detector. The receiving slit assembly and the detector are coupled to move around a circle in order to scan a range of 2θ(braggs) angles. For θ/2θ scans, the goniometer rotates the specimen about the same axis as the detector but at half rotational speed.

In this research the zinc oxide structural properties are studied with a Siemens D-500 powder diffractometer. The incident x-ray is copper K_α radiation and the scan range for 2θ is 25 degrees to 90 degrees.

4.1.2 Results and discussion from the XRD data

The electrochemical deposition is done on silicon substrate having zinc oxide as explained in section 3.2.4 of thickness of 10 micrometer and the XRD was performed on the

41

sample. Figure 4.1 shows the XRD spectrum of electrochemically deposited ZnO on silicon substrate. It shows zinc oxide peaks and the crystal orientation and it proves that this method produces zinc oxide.
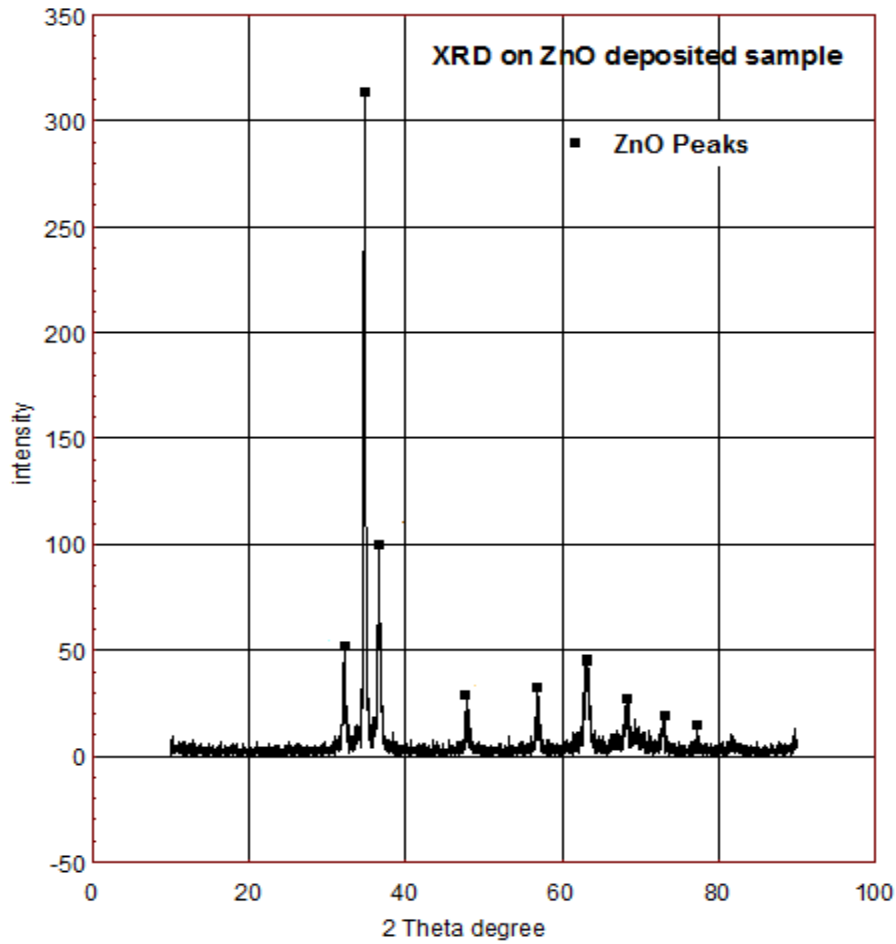

Figure 4.1 XRD spectrum of Zinc Oxide on Silicon Substrate.

4.2 Spectrophotometry and Band Gap Calculation of Zinc Oxide

4.2.1 Spectrophotometer

The change in intensity of light dI after passing through a sample should be proportional to path length, b, the longer the path, more photons should be absorbed; concentration, c, of the

sample, more molecules absorbing means more photons being absorbed; and intensity of incident light (I). The Beer-Lamberts Law,

$$A = \varepsilon bc$$

<div align="right">4.2</div>

where A is defined as the absorbance.

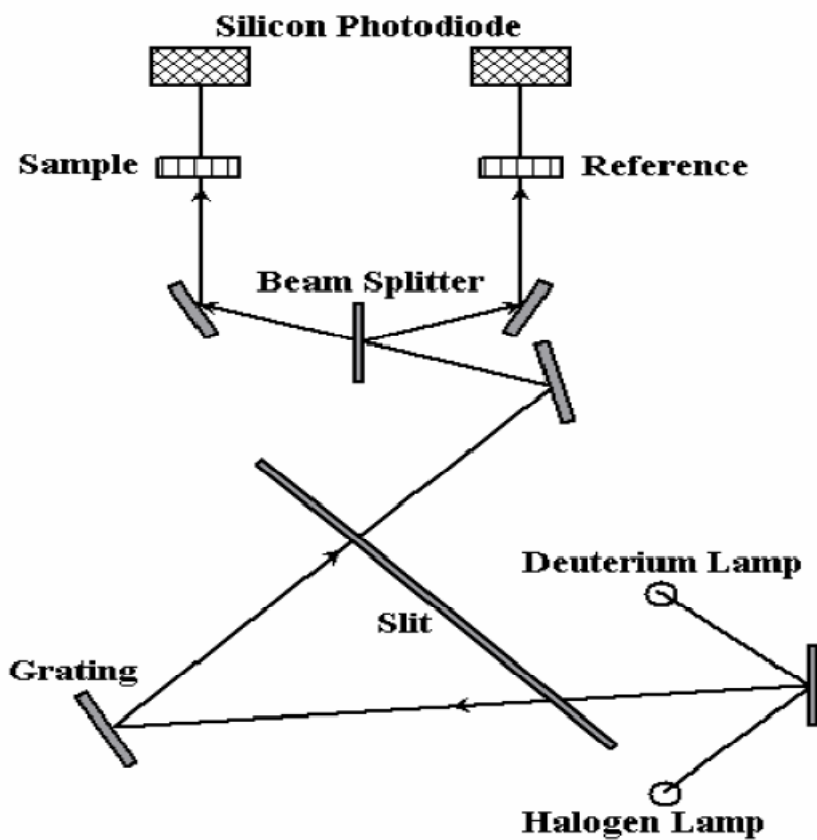All UV/VIS spectra is measured using Jasco UV/VIS V-570 and the schematic is shown below,

Figure 4.2 V-570 Spectrophotometer.

There are two light sources within a UV/VIS spectrophotometer. The visual light is generated by halogen lamp and the UV portion is generated by the deuterium lamp. Hence it gives a wavelength of 400nm to 1100nm of light. The light is then divided into two equal

intensity and passed through the test sample and a reference sample. A silicon photodiode is used to record the intensity of transmitted light.

4.2.2 Results and discussion

The band gap of zinc oxide is determined from the reflection and transmission data obtained from the electrochemical deposition of zinc oxide on the ITO surface.

The transmittance and reflection of ITO film is determined in advance before measuring the zinc oxide film. The plot of ITO and Zinc Oxide(ZnO) deposited transmittance is shown in figure 4.3. The specular reflectance(%) of ZnO on ITO is shown figure 4.4. To calculate the absorption coefficient, the thickness is zinc oxide was measured using profilometer and it was found to be 1.9µm and the absorption coefficient was found using the following formula,

$$\alpha = \frac{1}{t} \ln(\frac{1-R}{T})$$
4.3[45]

Where t is the thickness of the zinc oxide film and R and T are the reflectance and the transmittance respectively.
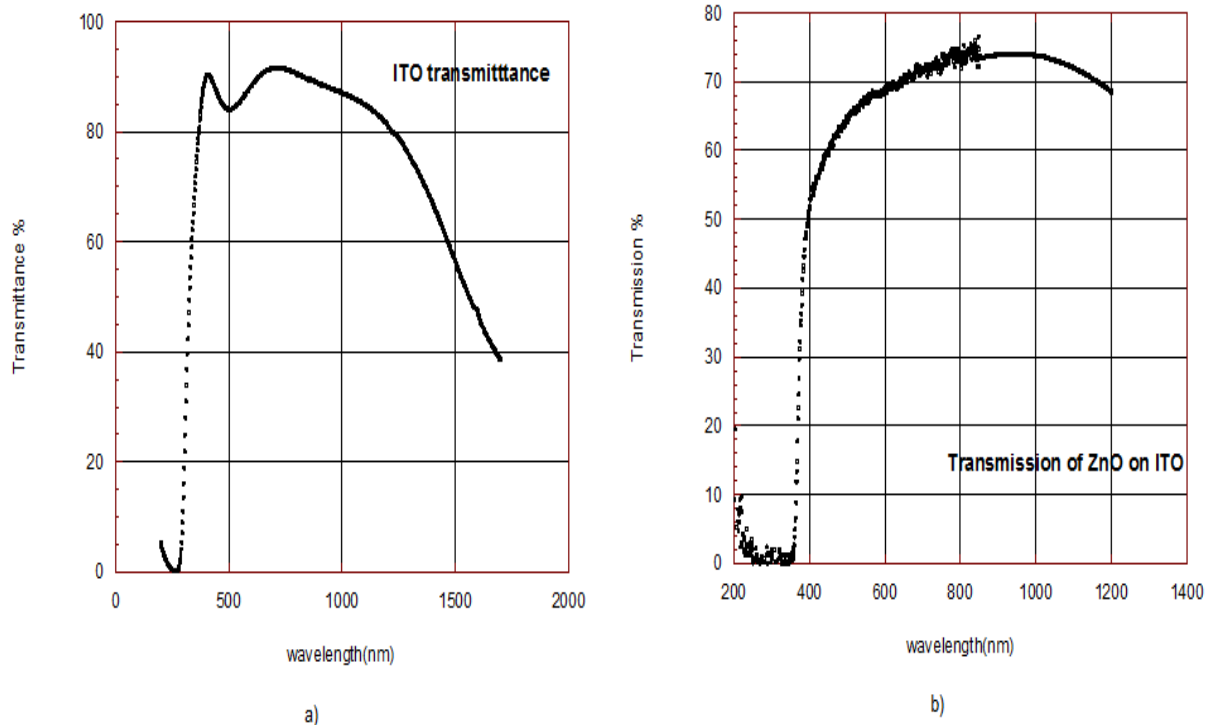
Figure 4.3 Transmittance of a) ITO b) ZnO/ITO

To calculate the optical band-gap energy, and the results were plotted using by the following equation:

$$(\alpha h v)^{p} = C\ (h v - E_{g})\qquad\qquad 4.4[47]$$

Where E_g is the band-gap energy and C is constant. The value of P is a power factor of 2 for direct bandgap and 0.5 for indirect band-gap. The different value of power factor P was reported for non-perfect crystal material such as amorphous [48].
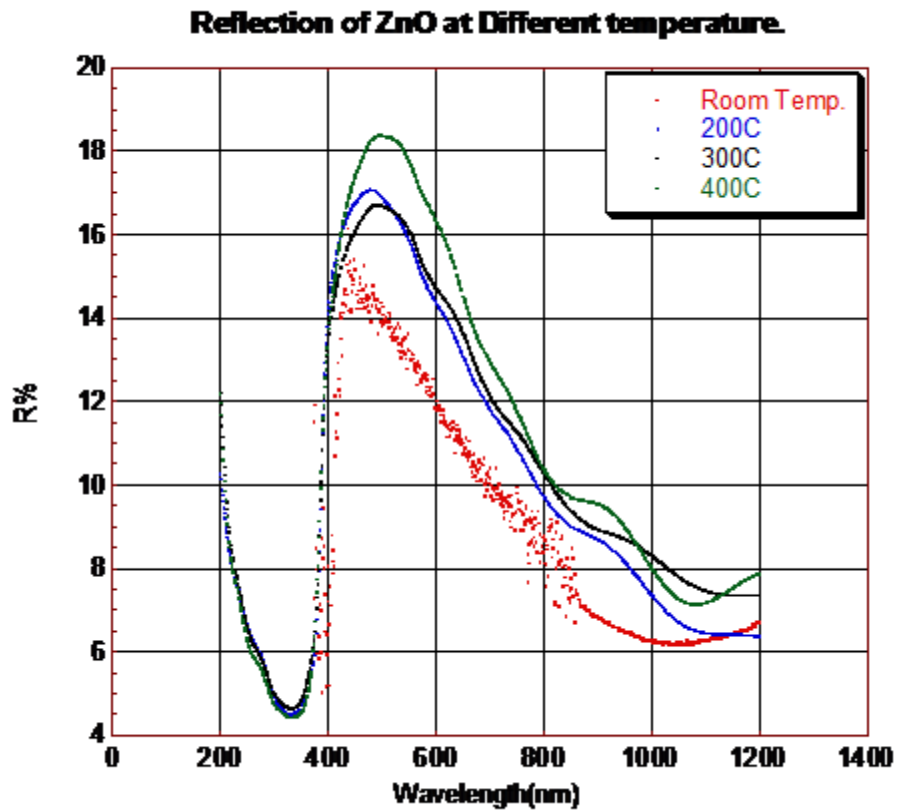
Figure 4.4 Reflectance(%) of Zinc Oxide.

The following figure 4.5 (a) shows the absorption coefficient of zinc oxide. The graph with $(\alpha h v)^P$ showed the best linearity with a value of 2 for P and hence the electrochemically deposited zinc oxide is a direct band-gap material. The figure 4.5 (b) shows the band-gap determination of the zinc oxide film which is found to be 3.36 eV.
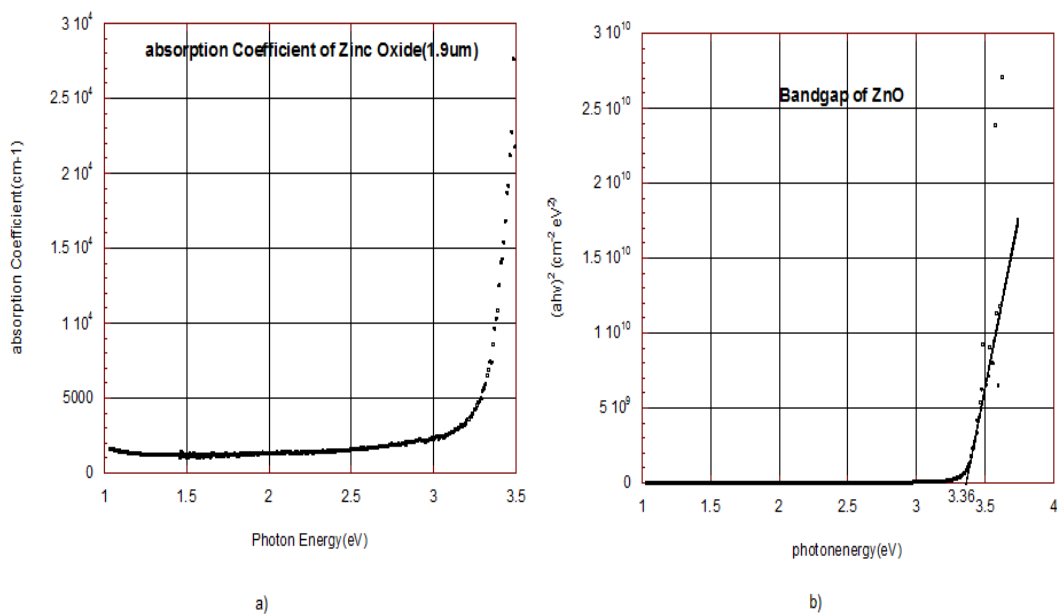
Figure 4.5 a)Absorption Coefficient of Zinc Oxide. b) Band-gap determination of ZnO

The transmittance and absorption coefficient at different annealing temperature was also measured and it is shown in figure 4.6 (a) and 4.6 (b) respectively. It is seen that that the transmittance increased after annealing at different temperature as also it can be seen the absorption coefficient also decreases as the annealing temperature is increased is from 400nm to 1200nm.
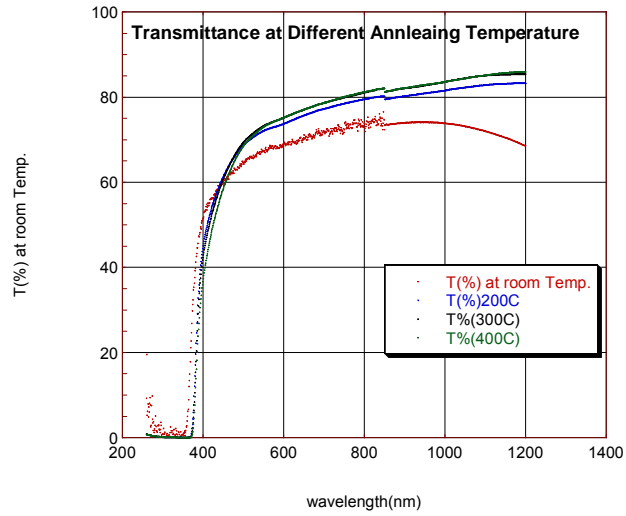
(a)
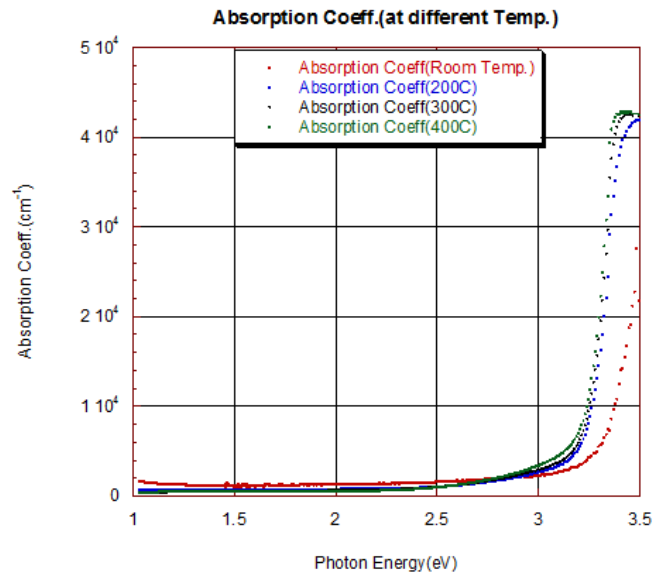
(b)

Figure 4.6 (a) Transmittance of Zinc Oxide at Different Annealing temperature. (b) Absorption Coefficient at Different Annealing Temperature.

4.3 SEM Characterization

The deposited zinc oxide is annealed at 400ºC for 30 minutes in open air before the extraction of the particles, shown in figure 4.7. A Hitachi S-3000N Variable Pressure SEM was used to characterize the particle image extracted from the Silicon mold, figure 4.9 to 4.11 shows the images of zinc oxide particles.
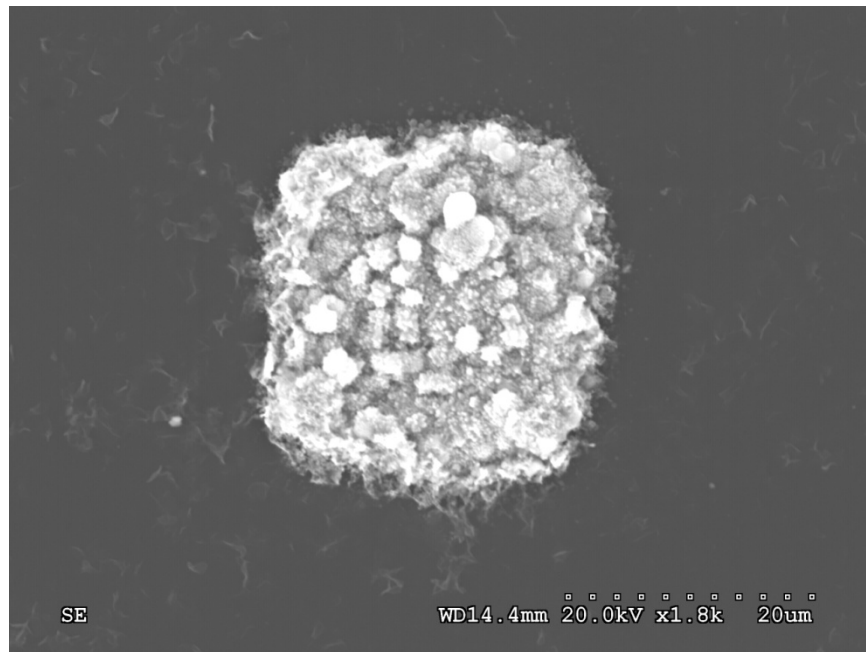
4.7. Annealed ZnO filled inverted pyramid.
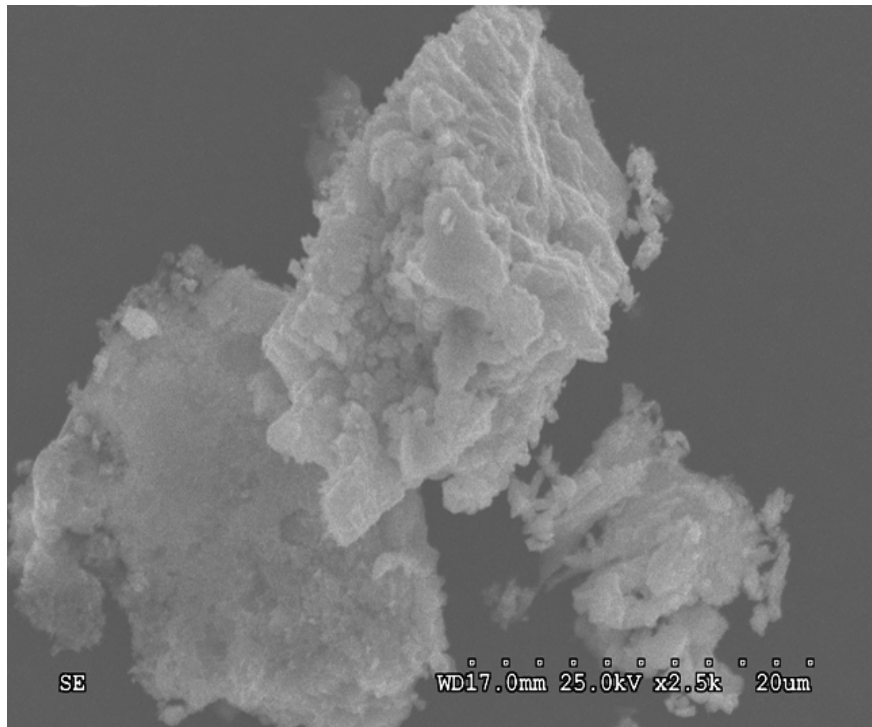
Figure 4.8 Extracted ZnO Particle
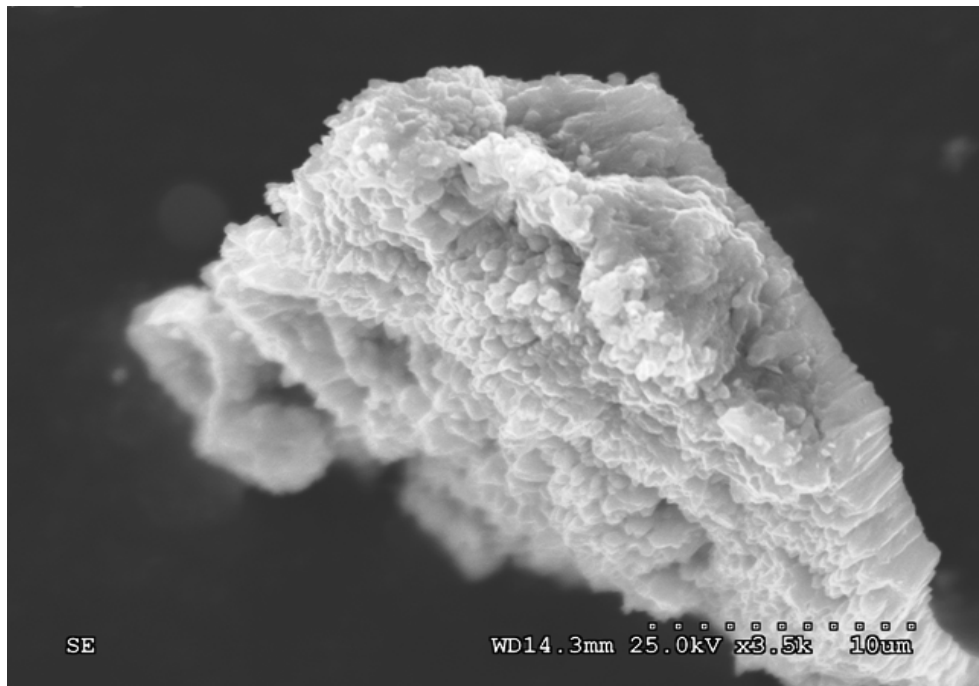
Figure 4.9 Extracted ZnO Particle
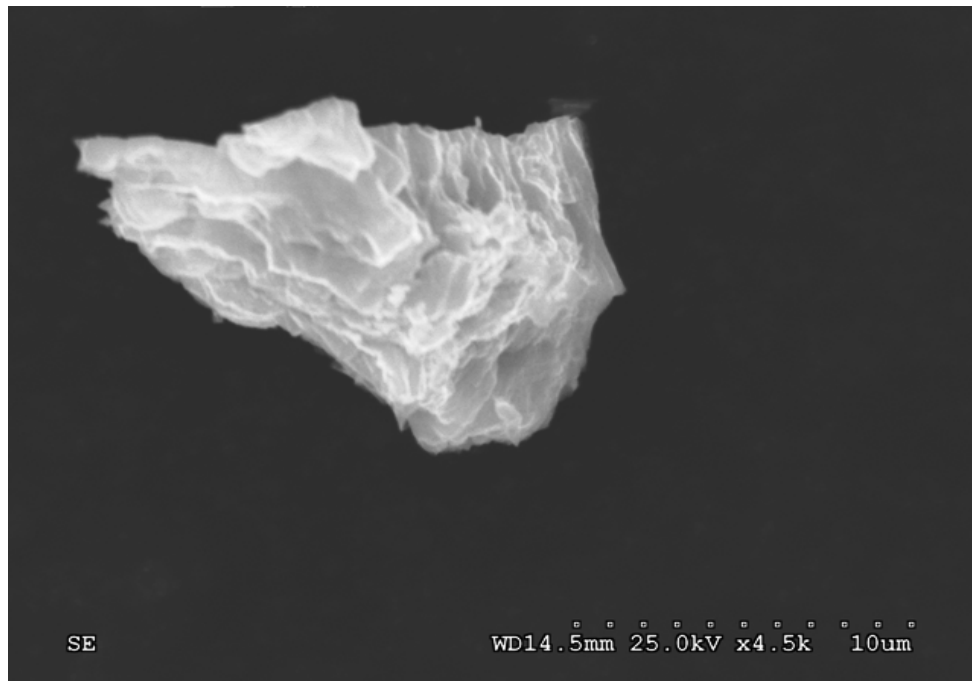
Figure 4.10 Extracted ZnO Particle
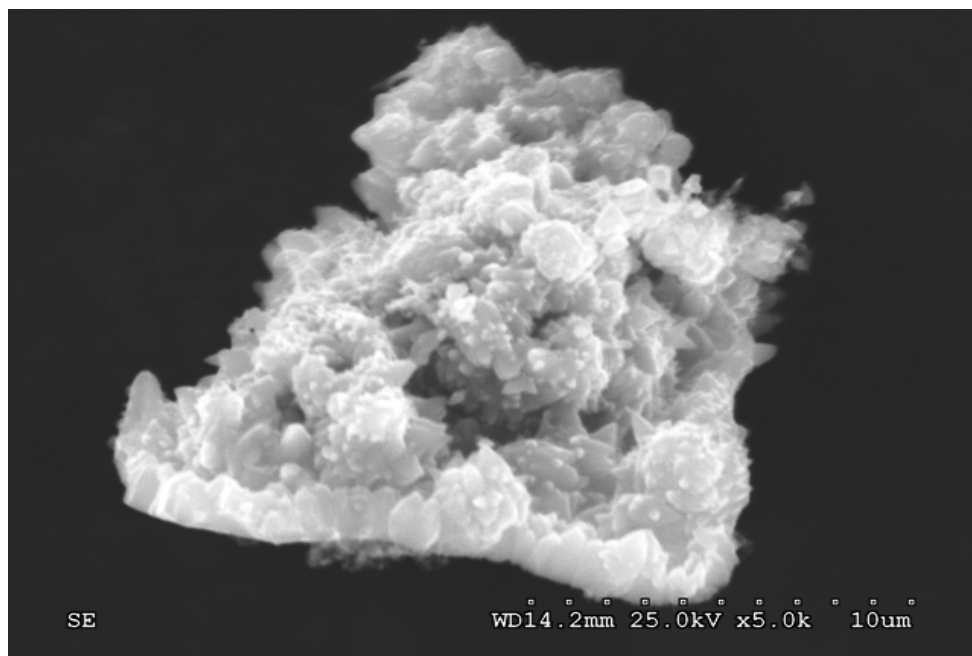
Figure 4.11 Extracted ZnO Particle

51

The definite shape of the particles is not easily obtained. The possible reason could be due to the difference in the thermal coefficient expansion of zinc oxide which is $\alpha_a = 4.31 \times 10^{-6}$ K^{-1} whereas silicon having the thermal coefficient expansion to be 2.6×10-6 K^{-1} and also there could a bond between silicon and zinc oxide which prohibits from getting a definite shape.

CHAPTER 5

CONCLUSION AND FUTURE WORK

5.1 Conclusion

Zinc Oxide is successfully deposited using the electrochemical method in the silicon mold and also structural and optical characterization is done and finally the zinc oxide particles are extracted.

Though it is difficult to obtain a definite shape with the above process method, still it signifies the fact that zinc oxide particles can be produced in a large scale using a cost effective method and which can be used for antireflective coating for solar cell.

5.2 Future Work

The main goal is to get the particular shape(in this case square pyramid) of zinc oxide keeping in mind the cost effective method. A high thermal expansion coefficient material mold (e.g. stainless Steel) can be used to deposit the zinc oxide and for the ease of extracting the particles from the metallic mold. Also research related to solution deposition like chemical bath deposition needs to be considered.

REFERENCES

[1] National Renewable Energy Laboratory.

[2] Friedolf M. Smits, Fellow, IEEE, "History of Silicon Solar Cells", IEEE transactions on Electron Devices, Vol. ED-23, ED-23, No. 7, July 1976.

 [3] Neville Richard C., " Solar Energy Conversion(The Solar Cell, Second Edition), Elsevier 1995.

[4] World Resources Institute (http://www.wri.org)

[5] Putnam P. C., "Energy in the Future" Rowman & Littlefield,Lanham, Maryland 1972.

[6] U.S. Energy Markets and Sumamry.

[7] BP Statistical Review of World Energy June 2009.

[8] U.S. Department of Energy, Basic Research Needs for Solar Energy Utilization(2005).

[9] Meng Tao, "Inorganic Photovoltaic Solar Cells: Silicon and Beyond", The Electrochemical Society Interface, Winter 2008.

[10] U.S. Department of Energy, Energy Information Administration(http://www.eia.doe.gov).

[11] Zwaan Bob van der, Ari Rabl, " The Learning potential of photovoltaics: implications for energy policy", Energy Policy 32,2003.

[12]Blokken Beddy, "Semiconductor Industry Steps Into the Solar PV Market", Director of Technology and Standards, SEMI Europe.

[13]http://www.semiconductor.net

[14] Deffree, Suzanne, "Photovoltaic Market to see 17% growth rate, Gartner reports, Electronic News Vol. 55 Issue 12, p1-1, 2009.

[15] Luque Antonio, Hegedus Steven, "Handbook Photovoltaic Science and Engineering",2002.

[16] V. Kapur, R. Kemmerle, A. Bansal,J. Haber, J. Schmitzberger, P. Le, D.Guevarra, V. Kapur, and T. Stempien, Conf. Rec. 33rd IEEE Photovoltaic Specialists Conf., IEEE, Piscataway, NJ (2008).

[17] B. Sang, F. Adurodija, M. Taylor, A. Lim,J. Taylor, Y. Chang, S. McWilliams, R.Oswald, B. J. Stanbery, M. van Hest,J. Nekuda, A. Miedaner, C. Curtis, J.Leisch, and D. Ginley, Conf. Rec. 33rdIEEE Photovoltaic Specialists Conf.,IEEE, Piscataway, NJ (2008).

[18] V. Bermudez, C. Ruiz, E. Saucedo, P.-P. Grand, and L. Parissikhaf, Conf.Rec. 33rd IEEE Photovoltaic Specialists Conf., IEEE, Piscataway, NJ (2008).

[19] D. B. Mitzi, M. Yuan, W. Liu, A.Kellock, S. J. Chey, A. Schrott, and V. Deline, Conf. Rec. 33rd IEEE Photovoltaic Specialists Conf., IEEE,Piscataway, NJ (2008).

[20] M. F. A. M. van Hest, C. J. Curtis, A. Miedaner, R. M. Pasquarelli, T. Kaydanova, P. Hersh, and D. S. Ginley, Conf. Rec. 33rd IEEE Photovoltaic Specialists Conf., IEEE, Piscataway, NJ (2008).

[21] M. Tao, W. Zhou, H. Yang, and L.Chen, Appl. Phys. Lett., 91, 81118 (2007).

[22] Van Der Ziel, Aldert, Solid State Physical Electronics (Englewood Cliffs, N. J.: Prentice-Hall,1976)

[23] Richard S. Muller,Theodore I. Kamins, "Device Electronics for Integrated Circuits, 3rd Edition", 2003.

[24] Van Zeghbroeck Bart, "Principles of Semiconductor Devices" 2007.

[25] Sze, S.M., "Physics of Semiconductor Devices" 2nd Edition, Wiley, 1981.

[26] M. P. Thekaekara, "Data on Incident Solar Energy" Suppl. Proc. 20th Annual Meeting Institute of Environmental Science 1974,p21.

[27] Bhattacharya Pallav, "Semiconductor Optoelectronic Devices", Prentice-Hall, Inc. 1994.

[28] Fonash Stephen, "Solar cell Device Physics" Academic Press, 1982.

[29] Mauk G Michael "Thin Film Silicon Solar Cell with optical Confinement and their fabrication by solution growth" University of Delaware, 1986.

[30] Benda Vitezslav, "Solar Cell Physics and Technology", Czech Technical University, Prague.

[31] Rolf Brendel, "Thin-Film Cryustalline Silicon Solar cells: Physics and Technology, WILEY-VCH, 2003.

[32] Joachim Muller, Bernd Rech, Jiri Springer,Milan Vanecek, " TCO and Light trapping in silicon Solar cells", Solar Energy, 2004.

[33] Xiaofei Han, Kun Hee Han, Meng Tao, "Electrodeposition of Group-IIIA doped ZnO as a Transparent Conductive Oxide" Electrochemical Transaction Society.

[34] Weidong Zhou, Meng Tao, Li Chen, Hongjun Yang " Microstructured Surface Design for Omnidirectional antireflective coatings on Solar Cells", American Institute of Physics, 2007.

[35] B. Dale and H.G. Rudenberg, "Photovoltaic Conversion, 1:High Efficiency Silicon Solar Cells", Proc. 14th Annual Power Sources Conf., US Army Signal Research and Develeopement Lab.,Ft. Monmouth, New Jersey, May, 1960, p. 22.

[36] H. G. Rudenberg and B. Dale, "Radiant Energy Transducer", US Patent 3,150,999, 1961.

[37] Patrick Campbell and Martin A. Green, "Light Trapping Properties of Pyramidal Textured Surface" J. Appl. Physics. 62(1), July 1987.

[38] F.E. Rasmussen, B. Geilman, M. Heschel, O. Hansen and A. M. Jorgensen, "Development and Characterization of KOH resistant PECVD Silicon Nitride for Microsystems Applications".

[39] A. K. Stamper and S. L. Pennington, "Characterization of Plasma-Enhanced Chemical Vapor Deposited Nitride Films used in Very Large Scale Integrated Applications", Journal of Electrochemical Society, Vol. 140, No. 6, June 1993.

[40] http://www.triontech.com/orion.htm

[41] Kenneth E. Bean, "Anisotropic Etching of Silicon" IEEE transactions of Electron devices, Vol. ED 25 No.10, 1978.

[42] Stanley Wolf, Richard N Tauber, "Silicon Processing for the VLSI Era" Volume I, Lattice Press 1986.

[43] A. J. Bard and L. R. Faulkner, Electrochemical Methods–Fundamentals and Applications, 2nd edition, John Wiley & Sons, New York (2000).

[44] Mosanobu Izaki, Takashi Omi "Characterization of Transparent Zinc Oxide Films prepared by Electrochemical Reaction", J. Electrochem. Soc. Vol. 144, No. 6, June 1997.

[45] Chennupati Jagadish, Stphen J. Pearton, "Zinc Oxide Bulk, Thin Films and Nanostructures", Elsevier 2006.

[46] B. D. Cullity "Elements of X-Ray Diffraction" Adison Wisley, 1967.

[47] Mark Fox, "Optical Properties of solids",

[48] Richard. L. Petritz, Phys. Rev., 110, 1254 (1958).

BIOGRAPHICAL INFORMATION

Amit Banik gained his Bachelor of Engineering from Visveswaraiah Technological University, Karnataka, India in 2005 with a major in Electronics and Communication Engineering. He joined The University of Texas at Arlington in Electrical Engineering(EE) Department for his Master of Science(M.S.) with Thesis option in 2007 and earned a M.S. degree in EE department in 2009.